Impact Damage Formation on Composite Aircraft Structures

Principal Investigator: Hyonny Kim*, Associate Professor

Student Researchers: Gabriela DeFrancisci, Zhi Ming Chen, Jennifer Rhymer, Sho Funai, Mac Delaney, Sarah Fung, Jacqui Le, and Sara White

Department of Structural Engineering, University of California San Diego
La Jolla, CA 92093-0085

Project Description Paper Supporting Presentation Given at
Federal Aviation Administration JAMS 2012 Technical Review Meeting
5 April 2012, Baltimore, MD

Abstract

The impact of composite structures from sources that involve wide area contact is of interest due to the tendency to produce internal damage with little or no exterior visibility. Specifically, impact by ground service equipment (GSE) having rubber-covered bumpers, high velocity hail ice impact, and impact by large radius metal tips are being investigated. Experiments representing GSE impact on a curved stiffened skin structure (five frames, four stringers) at a velocity of 0.5 m/s has shown complete failure of the three frames that were impacted. The exterior skin, however, exhibited no cracks and imperceptible levels of permanent deformation. Modeling methodologies are being established to predict the initiation and propagation of damage from GSE. Similarly, the modeling capability to predict impact damage from high speed ice impacts has been developed and threshold force-based failure criteria have been identified. Large radius metal tip impact-created dents are observed to relax considerably relative to a 25.4 mm diameter impactor tip.

* *corresponding author: hyonny@ucsd.edu*

1.0 Introduction

1.1 Motivation

Impact damage is an ongoing threat of major concern, particularly with the new generation of aircraft coming into service which have a significant percentage of their structure made of composites and are exposed to external sources of impact. This is a major concern due to the resilience of the composite outer skins which can sustain a high degree of deformation without developing cracks, even though the internal sub-structure is damaged. Thus, the traditional reliance on visual detection to find damage, which worked well for metal skins that dent easily, may be inadequate for composite airframes, particularly those having skin+stringer construction.

Focused investigations on the development of damage from blunt impacts are needed to address the difficulties that exist in being able to visually detect and predict the corresponding damage and to aid in assessing its effect on structural performance. The research conducted at University of California at San Diego (UCSD) has been focused on blunt impact sources that are not well understood. Topics of UCSD-focus are summarized in Figure 1 in the form of energy levels and damage sizes expected for the various impact sources being investigated. These topics are:

i. Impact/contact by ground service equipment (GSE) such as ground vehicles, cargo loaders, and any other equipment coming in close proximity to a commercial aircraft. GSE is a source of great damage potential due to the high mass of the GSE (typically 3,000 to 10,000 kg)

and subsequently high energies involved. Figure 1 shows the kinetic energy levels of GSE to be in the 10^2 to 10^3 J range (e.g., 10,000 kg cargo loader moving at 2 mph, or 0.894 m/s, has 4,000 J of kinetic energy). The length scale of contact for GSE impact can range from ~20 cm for a belt loader single D-shaped bumper, to over 2 m for a long cargo loader bumper (see Figure 1). It should be noted that ground service equipment (GSE) historically accounts for a major percentage of damage occurring to commercial transport aircraft [1], and is expected to continue to be a major source regardless of whether the aircraft is made from aluminum or carbon/epoxy composite.

ii. High velocity hail ice impacts involve high energy levels, exceeding 1,000 J (see Figure 1), mainly by virtue of typical aircraft in-flight speeds (well over 200 m/s). Even higher velocities (energy) are possible for rotating components like helicopter rotor and engine fan blades. Ground hail occurs at lower energy levels (velocity ~ 25 to 30 m/s) as depicted in Figure 1 for hail impacts. The ice projectile is complex in that it exhibits an initial elastic-type response and then severely crushes during the course of impact. This crushability results in a larger zone of contact, as shown in Figure 1, which significantly reduces the propensity to impart visual damage. Meanwhile, ice impact can produce large-area skin-stringer separation with no external visibility, unless penetration is achieved.

iii. Low velocity impacts by metal tips of large radius (up to 76 mm radius) are being investigated as a representation of impacts by generic sources,

such as dropped equipment, or contact with GSE features that are not covered by rubber bumpers, e.g., railings and rounded corners. The results of impacts by large radius tips are contrasted with a 12.7 mm radius (1 in. diameter) tip that is most commonly used for creating barely visible impact damage (BVID) of a specified dent depth (e.g., 0.3 mm). Such damage source, while commonly practiced as part of an airframe component's damage tolerance program, may not be representative of blunt sources of damage which can involve higher energy levels.

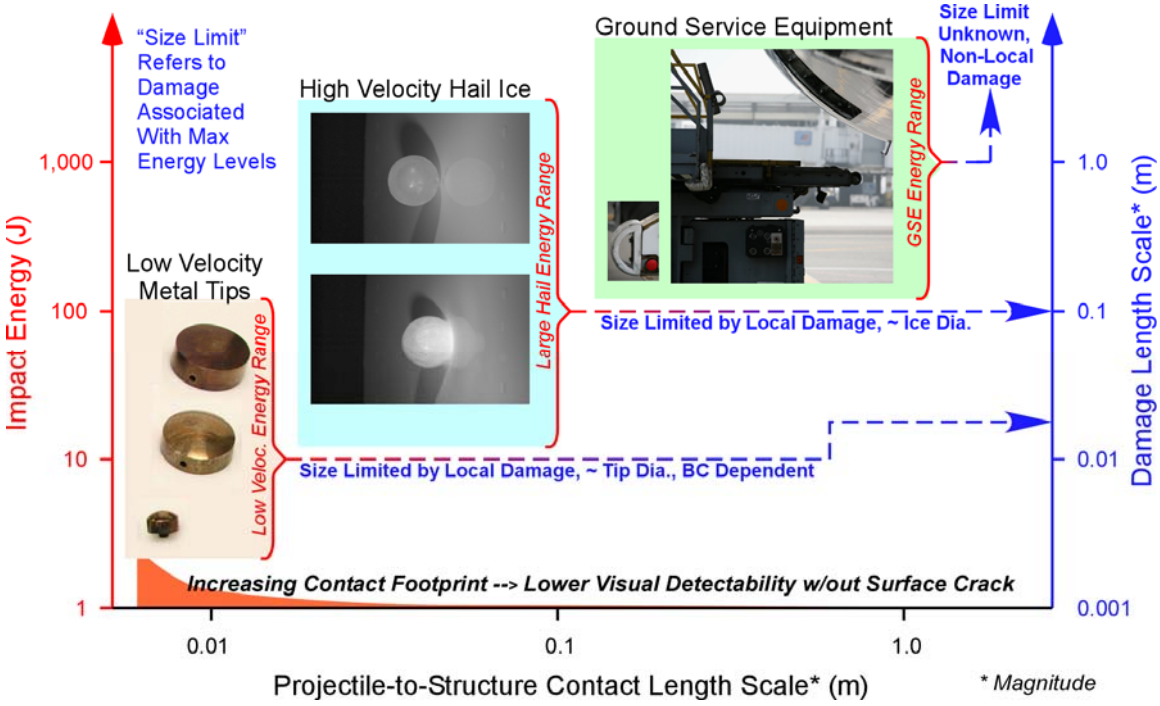

Figure 1. Blunt Impact Energy-Damage Spectrum

Extensive sub-surface damage usually forms when impacts occur at levels just exceeding the amount needed to initiate failure (Kim et al. [2], Kim and Kedward [3]), i.e., when the failure threshold is exceeded. Additionally, damage from blunt impacts to internal stiffeners can be extensive, existing in the form of

separation of stiffeners from the skin and fracture of the stiffeners. Of critical concern is whether damage is extensive enough to result in the structure losing ultimate and even limit load capability.

Among the three impact sources being studied (see Figure 1), both the low velocity metal tips and high velocity ice impact can usually be associated with a damage size limit. This damage limit reflects the ability for these impact sources to induce localized failure at the point of impact/contact. Thus, maximum-level cases of velocity and energy will typically produce penetration damage as a result of this localized response. Penetration damage has a size limit roughly equivalent in dimension to the impacting projectile. For the GSE impact, a non-local response has been observed to be possible. Specifically, internal damage can occur at locations away from the point of impact/contact, e.g., at joints or stress concentrations along the path of internal reaction. Thus, the damage size limit is not clearly known and, depending on the severity of the impact event, can be larger than the length scale of the contact between the projectile and structure.

1.2 Additional Background on Blunt Impacts

Blunt impacts can be defined as impact sources that can affect large areas or multiple structural elements, while potentially leaving little or no externally visibly detectable signs of damage. Blunt impacts come from a variety of sources and can involve a wide range of energy levels, as illustrated in Figure 1. Figure 2 shows the portions of the aircraft where such threats typically occur. The side and lower facing surfaces of the aircraft are subject to contact with

GSE, whereas all exposed upper and vertical surfaces are subject to ground hail impact (terminal velocity + wind gust) and forward-facing surfaces are subject to in-flight hail impacts. UCSD's activities on these areas are closely tied in with industrial activities and directly address aviation industry-driven needs for increased knowledge in these areas from both experimental and analytical/computational viewpoints, ultimately aiding in the development of more efficient and safe aircraft structures.

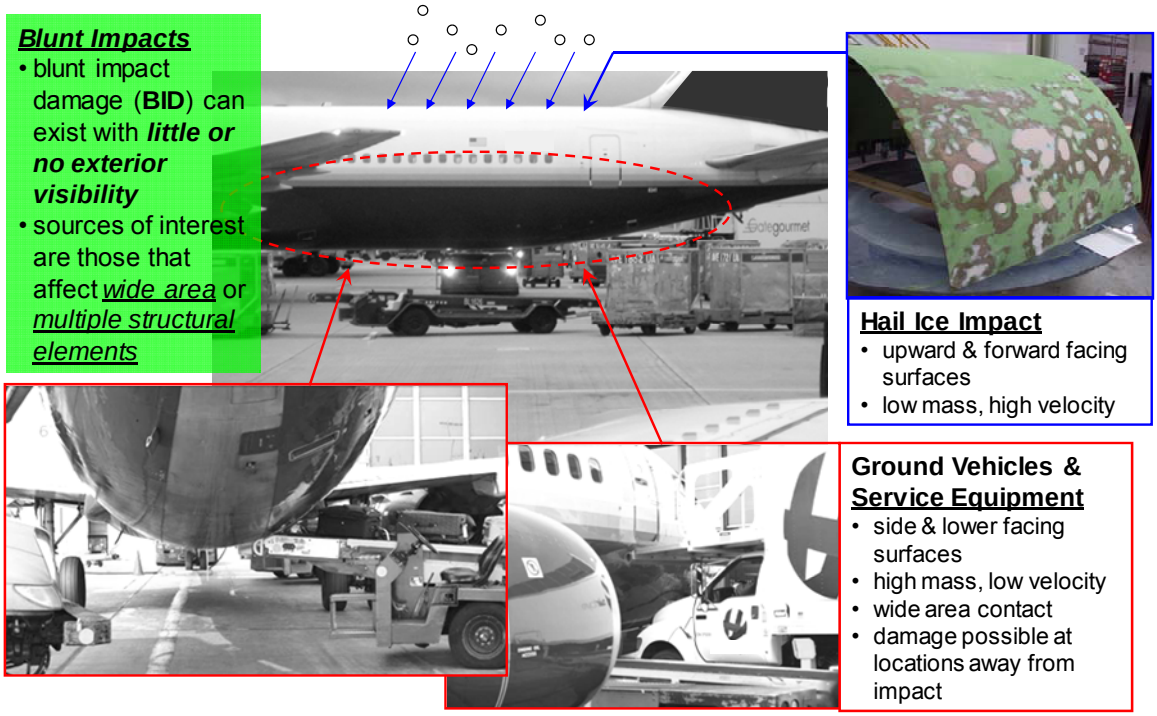

Figure 2. UCSD Blunt Impact Focus: Hail Ice and Ground Service Equipment

1.3 Objectives

The objectives of this research program focuses on impact damage formation by a range of sources, including: (i) low velocity wide-area blunt impact – vehicle/ground maintenance contact with composite aircraft structure, (ii) high

velocity hail ice impact, and (iii) impact by low velocity metallic tips of large radius. A common set of objectives exists for these three project focuses:

1. Characterize blunt impact threats and the locations where damage can occur.
2. Understand BID formation and visual detectability, specifically seeking to:
    - determine key phenomena and parameters,
    - understand how damage is affected by bluntness/contact-area,
    - identify and predict failure thresholds (useful for design), and
    - establish what conditions relate to development of significant internal damage with minimal or no exterior visual detectability.
3. Develop analysis and testing methodologies, including new modeling capabilities validated by tests. This would include defining how to analytically predict whether damage is visually detectable or not.

1.4 Approach

While each of the project focus areas has unique challenges related to their length scales and velocity regimes, a common general approach to achieve these objectives is the following:

1. Experiments: impact representative structure/specimens, specifically
    - wide area high energy blunt impact – e.g., from ground service equipment,
    - high velocity hail ice impacts – in-flight and ground-hail conditions, effect of internal stiffeners,

- low velocity impacts – non-deforming impactor, understanding large radius effects.

2. Modeling development – nonlinear FEA, analytical simple models, energy balance.
3. Communication of results to industry and collaboration on relevant problems/projects via workshops and meetings (at UCSD, via teleconf).

1.5 Expected Outcomes

Accomplishment of these objectives are intended to aid engineers in assessing whether an incident could have caused damage to a structure, and if so, what sort of damage mode, extent, and location such damage would occur. This information assists with understanding of what kind of inspection techniques should be applied to assess the extent of damage. Furthermore, it is expected that design engineers can make use of the research outcomes to: (i) improve the resistance of composite aircraft structures to damage from blunt impacts sources, and (ii) provide critical information on the mode and extent of seeded damage for use in damage tolerance considerations and definition of what is termed BVID.

1.6 Research Partners

UCSD's research on impact of composites is of direct interest to industry. The following Table 1 summarizes the research partners that are involved in the project with UCSD. Large and small aircraft manufacturers, a small composites-specialty engineering firm, and a material supplier are represented.

Table 1. UCSD Research Partners

Name of Persons/ Company	Description/ Expertise	Role in UCSD Project
Boeing	OEM – Large Transport Aircraft	Provide guidance and input on blunt impact. Particular focus on blunt impacts onto panels of stiffened-skin construction. Possibly supply test panels.
Airbus	OEM – Large Transport Aircraft	Provide guidance and input on blunt impact. Particular focus on blunt impacts onto panels of stiffened-skin construction. Possibly supply test panels.
Bombardier	OEM – Small/Regional Aircraft	Provide guidance and input on hail ice impact, particularly focused on sandwich panels. Supply test panels for ice impact.
Bell Helicopter	OEM – Rotorcraft	Provide guidance and input on hail ice impact, particularly focused on sandwich panels. Supply test panels for ice impact.
San Diego Composites	Composites Design and Manufacturing	Provide technical advice on the direction of the project, guidance on the design of the large-scale blunt impact composite test panels, guidance on the design of tooling for manufacturing the test panels, and access to large autoclave for curing panels.
Cytec Engineered Materials	Materials Supplier	Provide technical advice on project directions. Provide guidance on use of materials. Supply carbon/epoxy prepreg materials to support fabrication of test specimens at UCSD for both blunt impact and hail ice studies.
United Airlines	Airline	Provide guidance and feedback on project directions particularly with reference to operator view. Participate in on-site meetings.
Delta Airlines	Airline	Provide guidance and feedback on project directions particularly with reference to operator view. Participate in on-site meetings.
Sandia National Lab	National Lab – Nondestructive Evaluation	Conduct advanced non destructive investigation (NDI) on impacted test panels to aid in understanding of damage extent developed, and determine detectability of non-visible damage modes.
JCH Consultants	Consultant on Aircraft Safety and Composites	Advise on direction of project, provide guidance on tests, data reduction, results interpretation and dissemination to the public and senior-level individuals in industry as well as to military (Air Force).

2.0 Wide Area Blunt Impact Damage

2.1 Background and Motivation

With the increased use of composites in airframe primary structural components (e.g., fuselage and wing), there is a need to better understand the damage mechanisms caused by accidental transverse impact loading,

particularly for high energy levels. The largest source of damage to a commercial aircraft is caused by accidental contact with ground service equipment (GSE). Specifically, 50% of *major* damage was recorded to be caused by baggage vehicles and 60% of *minor* damage was caused by collision with ground vehicles and equipment (International Air Transportation Association [1]). Typical GSE speeds between flights have been quantified (during UCSD visit to LAX) and it was found that GSE speeds up to 1 m/s were realistic within close proximity of the aircraft. The low velocity, yet large mass of the GSE involved results in high energy levels in the range of 250 to 1,500 J for typical belt loader traveling at speeds of 0.5 to 1 m/s (mass in range 2,000 to 3,000 kg). Heavy cargo loaders are several times higher in mass and will impart proportionally higher energy.

2.2. Summary of Previous Results

Quasi-static indentation tests were conducted on two series of test specimens similar to large transport aircraft fuselage sections. The StringerXX series tests are intended to help understand blunt impacts that occur in between frames, and the FrameXX series tests are similar to blunt impacts caused by loading across multiple frames. Detailed descriptions of specimen designs and experimental setups, can be found in previous UCSD JAMS 2010 and 2011 review presentations and project papers.

Up until March 2011, five StringerXX specimens and two FrameXX specimens were tested with the indentor types and locations summarized in Table 2. The conclusion was drawn from these tests that indentation with a rubber indentor applied on the skin spanning between the stringers produces

wide spread internal damage to the panel and no externally visible signs of damage occurring. This is possible because the indentation does not produce high shear stress on the panel skin and the bending stresses did not exceeded failure levels to produce visible cracks. The rubber indentors reduce the high interlaminar shear stress at the point of contact, thus reducing the propensity to form localized delaminations. In contrast, indenting the specimens with an aluminum indentor at a position centered on top of stringer or at a stringer flange with a rubber indentor both produce externally visible cracks.

Table 2. Blunt Impact Tests as of March 2011 (as of 2011 JAMS Review)

Specimen ID	Panel Config	Loading Details (Q.Static Unless Noted)	Intermediate Failure Modes	Final Failure Mode	Vis-ible ?	Max Load (kN)	Max Displ (mm)
Stringer00	3 Stringers	R3" Alum. at Stringer	Skin Delamination	Local Skin Penetration	Y	30.7	25.3
Stringer01	2 Stringers	R3" Alum. on Skin Between Stringers	Skin Delamination	Local Skin Penetration	Y	26.7	21.8
Stringer02	2 Stringers	D-Bumper on Skin Between Stringers	Skin-Stringer Delamination of Each Adjacent Stringer	Extensive Stringer-Skin Delamination	N	61.7	39.5
Stringer03	3 Stringers	D-Bumper at Stringer	Stringer Radius Cracks Under Indentor	Extensive Stringer-Skin Delamination	Y	61.6	48.5
Stringer04	3 Stringers	D-Bumper on Stringer Flange	Stringer Radius Cracks Under Indentor	Extensive Stringer-Skin Delamination	Y	78.2	44.2
Frame01	4 Stringers, 3 Frames	Long Cyl. Bumper Between Stringers	Shear Ties Crush, Stringer Sever & Flange Delam	Frame Crack	N	57.4	75.5
Frame02	5 Stringers, 3 Frames	Long Cyl. Bumper at Stringer	Shear Ties Crush, Stringer Sever & Flange Delam, Skin Crack	Frame Crack	Y	71.0	55.9

The types of internal damages observed thus far include delamination of stringers from the panel skin and shear tie delamination/crushing for the StringerXX specimens. Severed shear ties, fractured frames, severed stringer were observed for the FrameXX specimens. A progressive damage process was

observed for the FrameXX specimens with frame rotation playing a major role in the process.

2.3 Recent Results

2.3.1 StringerXX Specimens – Experimental Results

The StringerXX specimens are smaller sized panels having skin, stringers, and shear ties with no frames. Shear ties are mounted directly to test boundary conditions in lieu of frames.

In the last year, two StringerXX specimens were tested. Test specimen Stringer05 (2-stringers, impacted between stringers) and Stringer06 (3-stringers, impacted on center stringer) have been dynamically tested with a D-shaped, OEM rubber bumper at a velocity of 0.5 m/s. The test setups for the two specimens are similar to prior StringerXX tests documented in Table 2. During both tests, the back of the bumper displaced 114.3 mm into the panel, creating significant skin cracks, panel stringer-to-skin delamination, and stringer flange/radius cracks. Post-test photos of Stringer05 with damages are shown in Figures 3 and 4 respectively.

A high speed camera running at 5000 fps was used to observe the bottom side of the panel during the experiment. The high speed video shows that as the panel is loaded, the skin-stringer delamination occurred first, followed by the stringer radius failure within 4 milliseconds. It is unknown when exactly the skin cracking occurred relative to the other failure events as that damage occurred outside the camera's field of view.

The Stringer05 load vs. actuator displacement plot is shown in Figure 5, along with the plot for Stringer02, a panel with the same dimensions and boundary conditions loaded quasi-statically. Two significant load-drops are shown in the Stringer05 loading curve, each is caused by skin-stringer delamination and stringer radius failure on one of the stringer flanges adjacent to the bumper loading zone. The first load drop occurred at 98 mm of actuator displacement. This load drop is surmised to be caused by failures on the stringer flange to the right of the bumper loading location. Although this flange is not shown in the high speed video, some debris can be seen ejected from that location during that time. The second load-drop occurred at 101 mm of displacement and was caused by failures near the flange to the left of the bumper. This was confirmed by the high speed video.

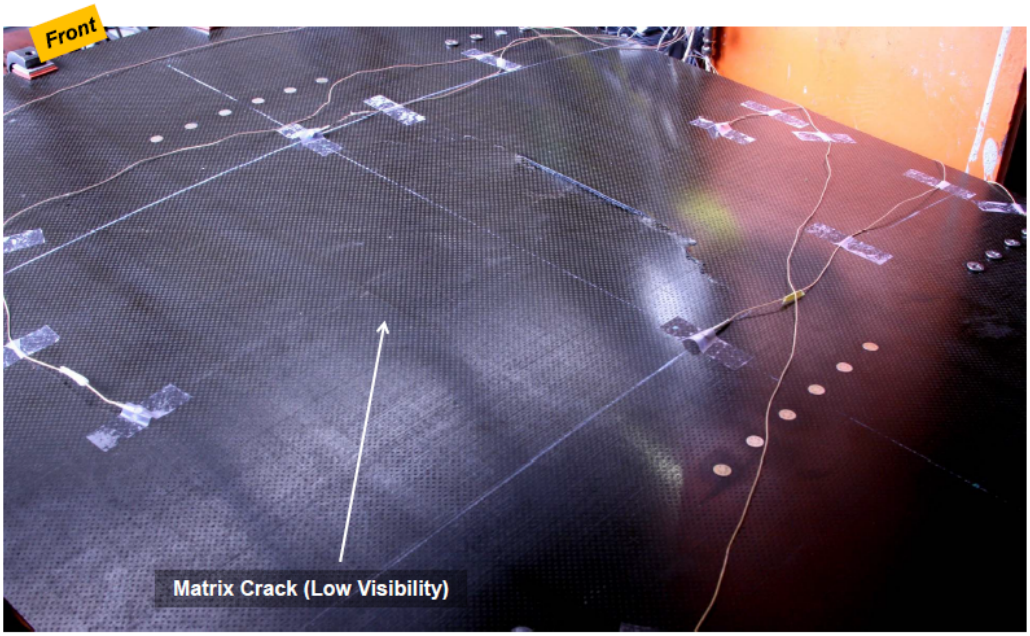

Figure 3. Post-Test State of Stringer05 Showing Surface Cracks Along the Stringer Radius Locations Adjacent to the Impact Location

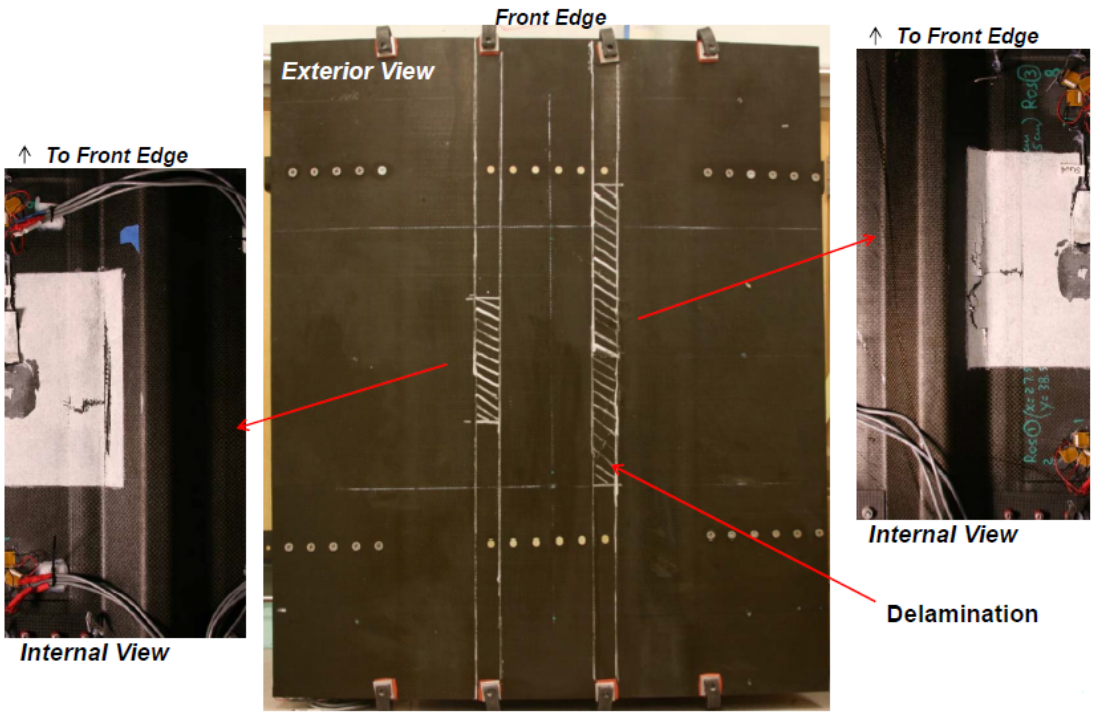

Figure 4. Center Image: Post-Test A-Scan Map of Stringer05 (Hatched Area = Skin-Stringer Delamination); Side Images: Crack Formations along the Stringer Radii and on the Flanges Viewed from Panel Inside

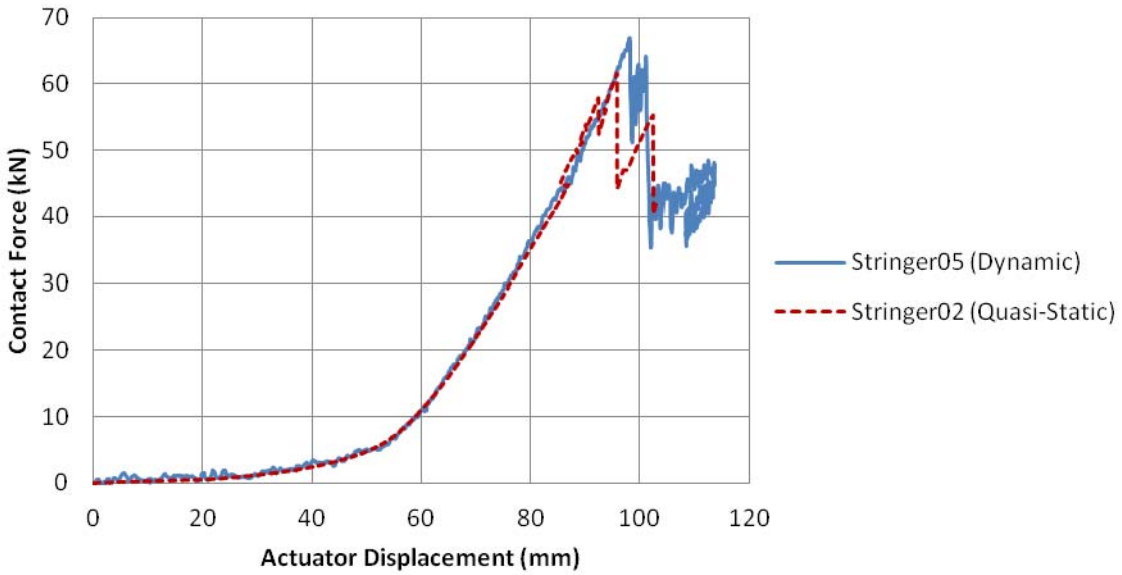

Figure 5. Stringer05 and Stringer02 Contact Force vs. Actuator Displacement

The post-test damage states for Stringer06 (3-stringers, impacted on center stringer) are very similar to that of Stringer05 shown in Figures 3 and 4. The Stringer06 load vs. actuator displacement plot is shown in Figure 6, along with the Stringer03 (i.e., same 3-stringer panel tested at quasi-static speed) data. Similar to the Stringer05 test, there are two incidences of significant load drops in the Stringer06 curve. Also, as confirmed by the high speed camera video of this test, each load drop corresponds to the stringer-to-skin delamination and stringer radius failure at each flange of the impacted stringer.

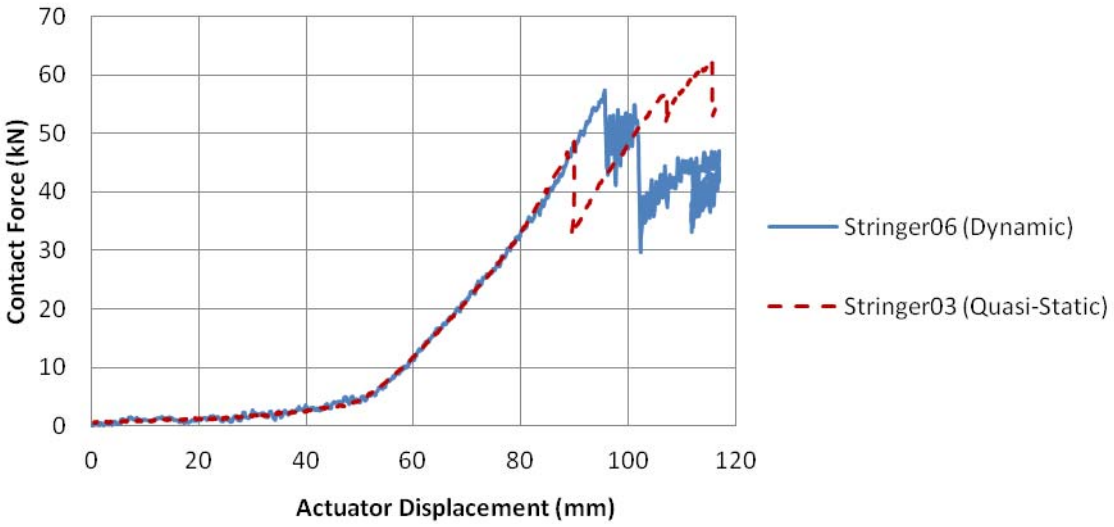

Figure 6. Stringer06 and Stringer03 Contact Force vs. Actuator Displacement

FEA simulations of the Stringer05 test was created with a D-shaped OEM bumper, as well as a flat rubber pad (to simulate a pre-collapsed bumper). The FE model of Stringer05 dynamic test included cohesive surfaces between the panel skin and stringer flanges to predict delaminations caused by interlaminar shear and tension stresses, and the Hashin-Rotem failure criteria was used to predict failure of the composite lamina caused by in-plane stresses. The final

failure state of the Stringer05 model (plotted as a map of the delaminated area) is shown in Figure 7 and compared with the post-test A-scan photo of the Stringer05 specimen. The figure shows that the simulation is an accurate representation of the test as the skin-stringer delamination is confined to the stringer flanges adjacent to the impacting zone, in the space between the shear ties.

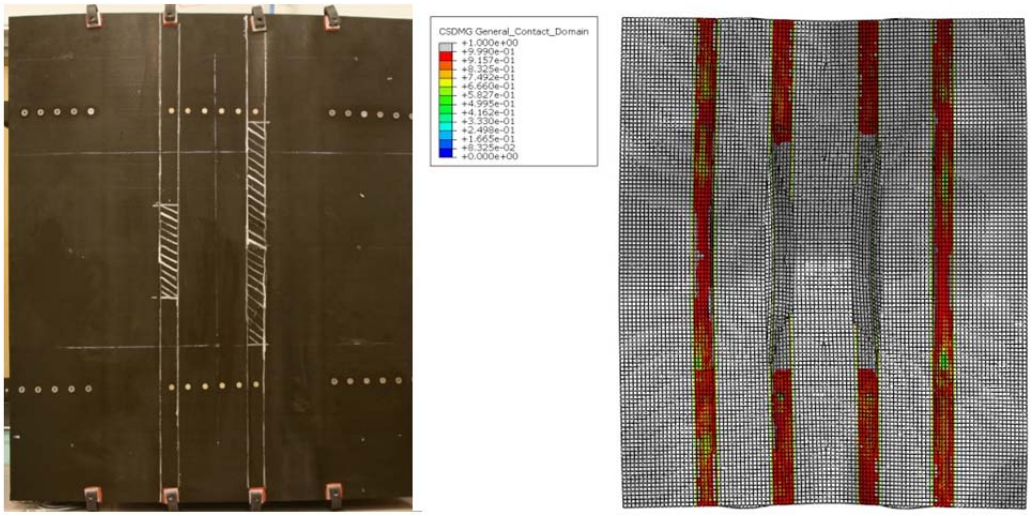

Figure 7. Comparison between the Post Test A-Scan Map of Stringer05 (Left) and the Final Delamination Map of the Stringer05 FE Model (Right; Red Zones Indicate Skin-Stringer Bond, Grey Zones Indicate No Bond)

2.3.2 FrameXX Specimens – Experimental Results

The FrameXX specimens are larger-sized specimens composed of skin, four stringers, and five frames connected to the skin via mechanically-fastened shear ties. Two of these specimens have been fabricated, referred to as Frame03 and Frame04.

The first five-frame specimen (Frame03) was tested in early March 2012. The 1 m long cylindrical rubber bumper was centered over the middle three

composite C-frames as shown in Figure 8 which also gives an overview of the general lab set up. Boundary conditions, as visible in Figure 8, include rotating end supports for each frame with controlled rotational stiffness achieved via flexure plates.

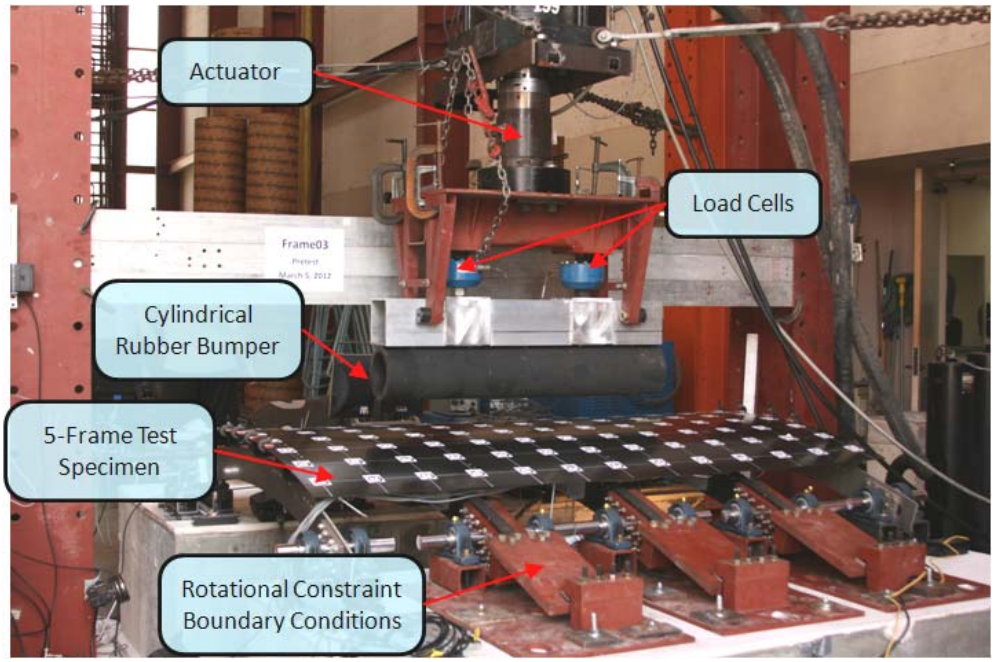

Figure 8. Test Set-up for Specimen Frame03

Loading was applied by a dynamic servohydraulic actuator onto which the 1 m long bumper was mounted. The specimen was loaded two times (referred to as L1 and L2) under displacement control, each with a constant velocity of 0.5 m/s, followed by a 0.5 s pause before unload. As shown in Figure 9, loading L1 had a total actuator displacement of 159 mm, which includes closing the initial gap of 6.4 mm. Moderate crushing damage in the radius area of the shear ties directly under the impactor occurred, but there was no delamination between the skin and stringers or shims. The cylindrical bumper has a hollow inner diameter

of 127 mm and so the expected displacement of the specimen surface was on the order of 25 mm.

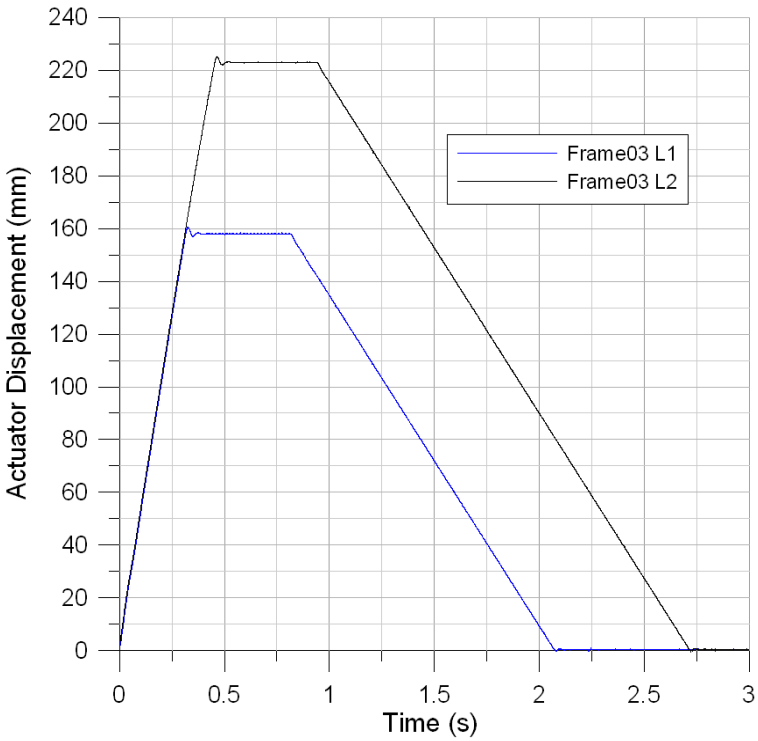

Figure 9. Frame03 Displacement Controlled Loading Histories

The total displacement of the actuator in the second Loading L2 was 222 mm, as shown in Figure 9. This loading caused extensive damage to the internal structure that is not visually detectable from the skin side (no visible cracks formed). All three C-frames were completely severed (each in two locations away from the impact location). Figure 10 shows a sequence of high speed video still captures that gives insight into the failure process. Upon complete crushing of the middle three (directly loaded) shear ties (see image 1 of Figure 10), the load was then transferred from the stringer directly to the C-frames (see image 2 of Figure 10). This is confirmed by the scraping marks observed on the stringers

and C-frames. As the impactor displacement increased, the C-frames rotated further, scraping along the stringer, leading to failure of the outer set of shear ties (see image 3 of Figure 10). Final failure occurred in the C-frames away of the impact region (i.e., non-local failure) due to a combination of torsion, bending and shear (see image 4 of Figure 10).

The final internal damage state is shown in Figure 11 and a view of the outside of the specimen after impact is shown in Figure 12. It should be noted that even after the frames were severed, the specimen still held a load of ~15kN per frame before unloading. While no immediately obvious damage is visible (i.e., no gross cracks), a minor surface geometry change was noted. The photogrammetry method was used, as summarized in Figure 13, to measure a 4.5 mm permanent deformation (relaxed state measured over 24 hours following test). The visual detectability of 4.5 mm acting over a “dent span” of 1 m has been found to be difficult to perceive by casual observation.

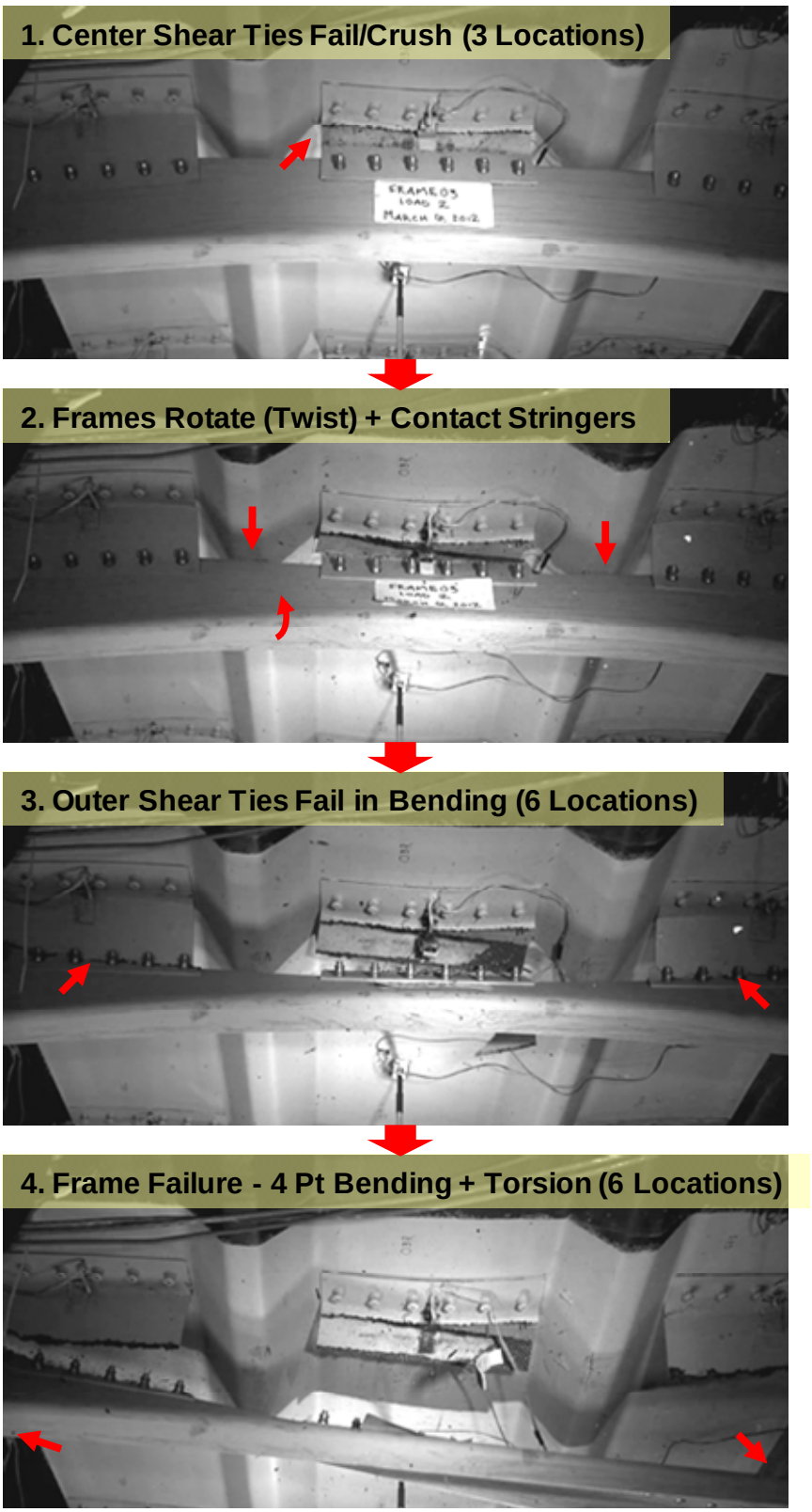

Figure 10. High Speed Video Stills Showing Sequence of Failure in Frame03

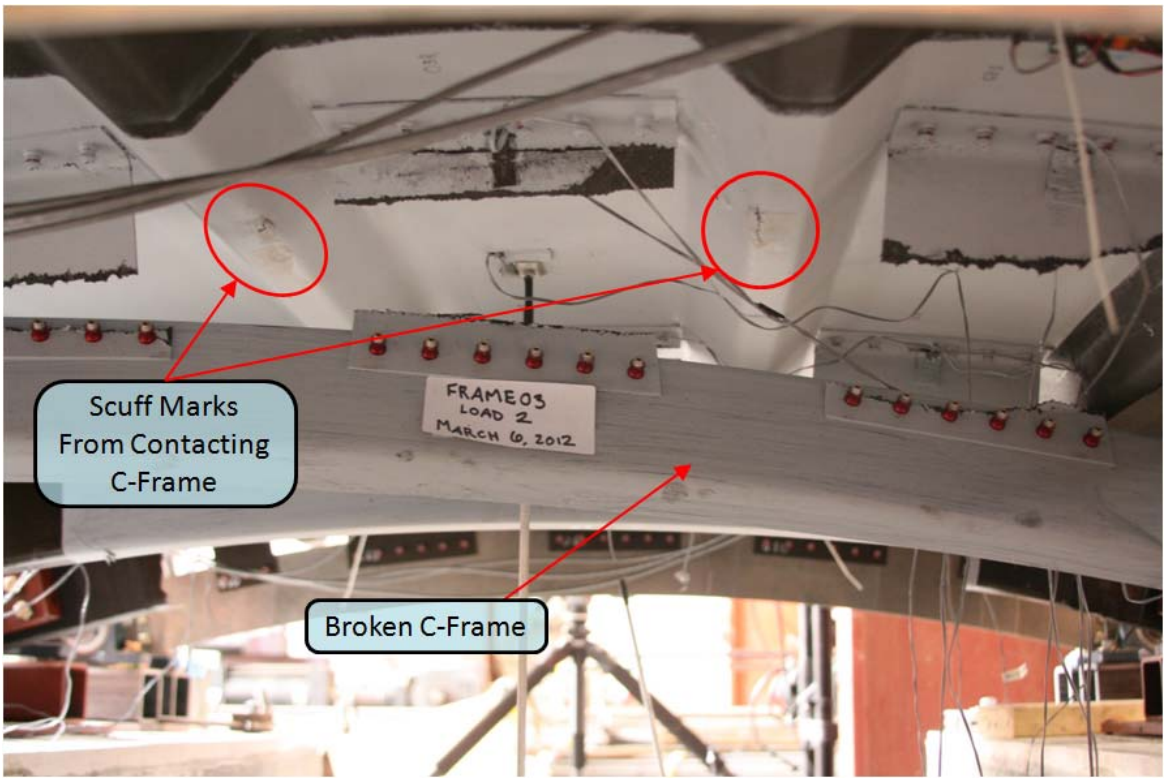

Figure 11. Frame and Shear Tie Damage of Frame03 after Loading L2

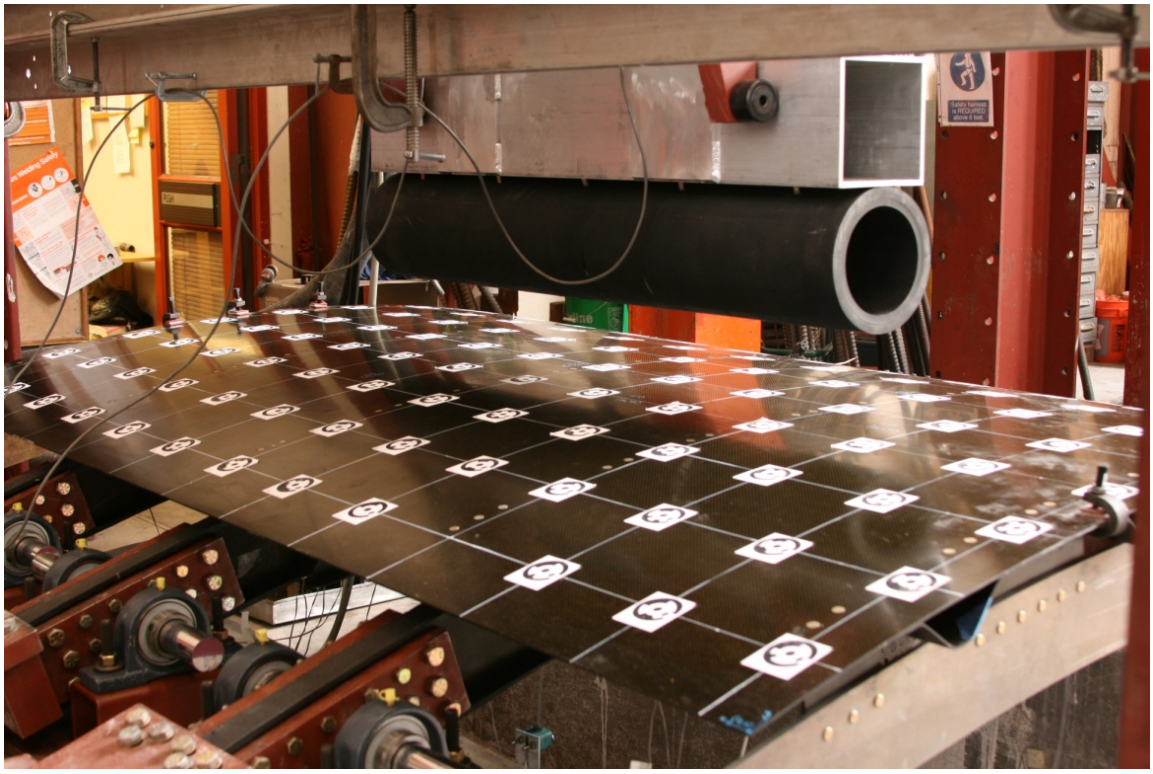

Figure 12. Frame03 after Loading L2

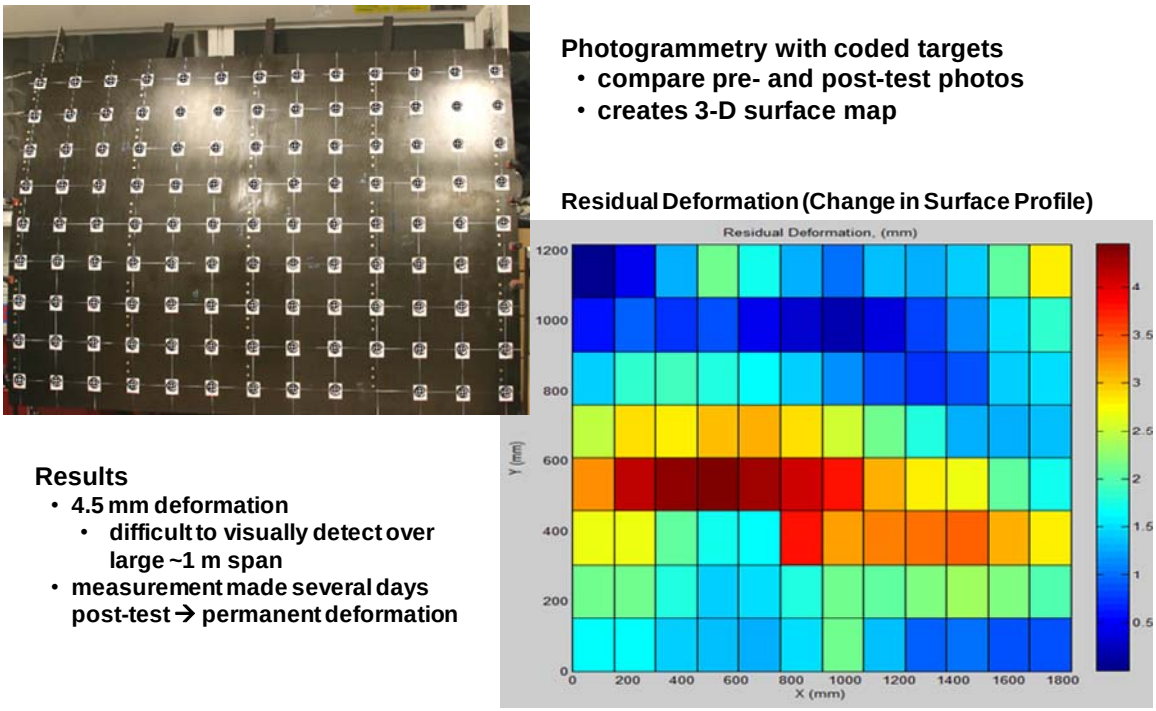

Figure 13. Frame03 Photogrammetry Measurement of Residual Geometry Change Following Loading L2

2.3.3 Sensor-Based Detection of Active Damage Events

Nondestructive sensor-based location of damage in panels for low velocity impacts using piezoelectric macro-fiber composite (MFC) strain gauges is currently being explored. Voltage response of MFCs are dependent on incoming wave angle so three MFCs can be used to determine longitudinal, transverse, and shear strain ($\bar{\varepsilon}_{xx}$, $\bar{\varepsilon}_{yy}$, $\bar{\gamma}_{xy}$). Using a rosette of three sensors, the three unknowns and incoming wave direction (φ) can be determined by the following equation:

$$\tan 2\varphi = \frac{\bar{\gamma}_{xy}}{\bar{\varepsilon}_{xx} - \bar{\varepsilon}_{yy}}$$

With a minimum of two rosettes, each providing an incoming angle, the intersection of the two lines projected at the angle from each rosette can be considered to be the wave source location.

Four rosettes were placed on specimen Frame03 which was impacted with a large rubber bumper. LabVIEW software was used to record the signals along with 20kHz - 2MHz analog filters to reduce noise and low frequency vibrations of the panel. This filtered signal focuses more on high frequency damage related information. Figure 14 plots the MFC signal results from the test. Each spike in voltage indicates the occurrence of a major event where some damage formation has occurred. While data processing is ongoing, the goal is to separately target each damage event and determine its location. Issues that arise include picking up signals from edge reflections, determining the transfer of high frequency signals through the shear ties and c-frames into the skin where it is received by the sensors, and distinguishing between separate events. Algorithms are being tested to resolve these problems, such as using threshold crossings to determine when one event has ended and a new event has begun.

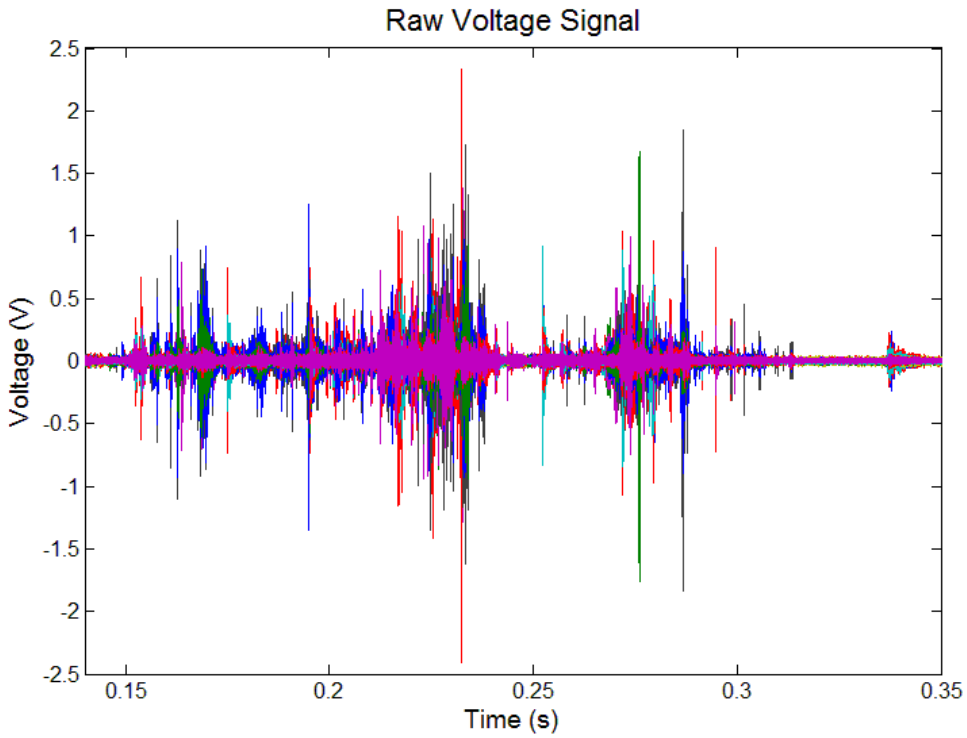

Figure 14. MFC Signal Measurement Showing Multiple Events During Test

2.4 Discussion

2.4.1 StringerXX Specimens

As shown in Figure 5, the initial stiffness of specimen Stringer05 (dynamic) is identical to the initial stiffness of Stringer02 (quasi-static). However, the Stringer05 dynamic test contrasts with the Stringer02 quasi-static test because damage is clearly visible from the exterior loaded surface. Also, dynamic impact has produced localized damage due to a dynamic localization effect when the panel was loaded quickly. Stringer05 experienced localized damage, as indicated by the cracks found underneath the impactor and the presence of localized delamination. On the other hand, Stringer02 showed no skin or stringer cracking, but more extensive skin-stringer delamination.

Similar to specimens Stringer05 and Stringer02, the initial stiffness of Stringer06 (dynamic) matches with Stringer03 (quasi-static). Damage for Stringer06 and Stringer03 were both localized underneath the impactor.

The contact force vs. actuator displacement plots of the Stringer05 FEA simulations and the experimental result are shown in Figure 15. As can be seen from this figure, the flat rubber pad simulation result (with offset displacement) matches up with the D-shaped bumper simulation result after the latter has fully collapsed. This validates the use of the flat bumper model as an approximation of a full D-shaped bumper, which is more computationally expensive to run and can lead to numerical instabilities. Also, the plots show that the FEA model, despite being stiffer than the actual experiment, accurately predicts the onset of each of the two skin-stringer delamination failures (accompanied by surface crack formation), as well as its resulting major load drops. For both delamination failures, the FEA-predicted peak loads are within 5% of the experimental data.

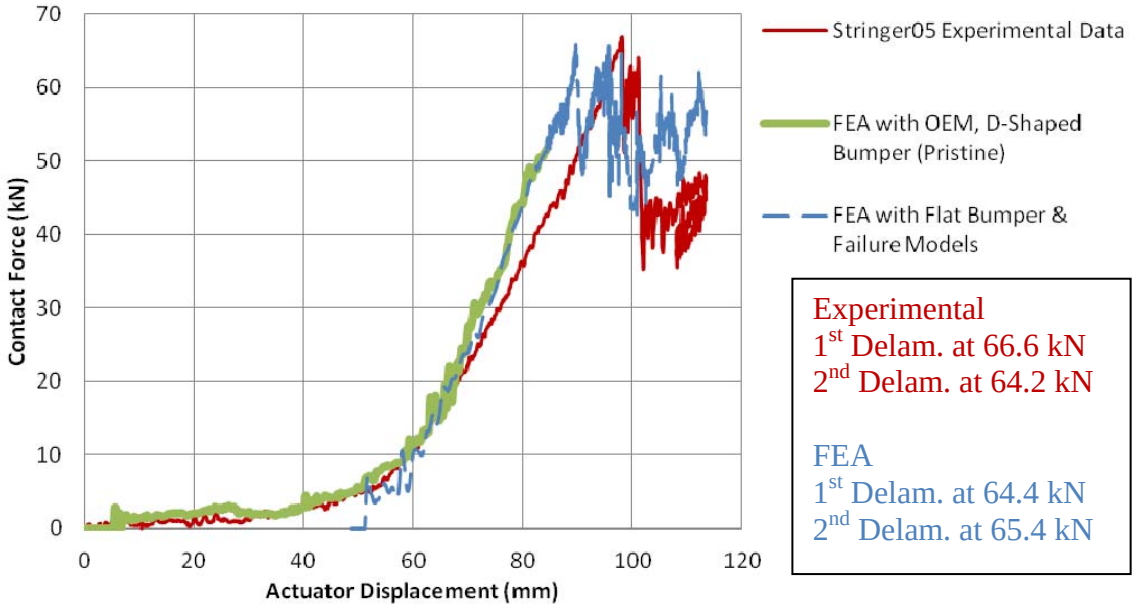

Figure 15. Contact Force vs. Actuator Displacement for Stringer05

2.4.2 FrameXX Specimens – Experiments

A force per frame-displacement comparison for quasi-static indentation and dynamic impact (Frame01 vs. Frame03) is shown in Figure 16. The initial stiffness of Frame03 (dynamic) is slightly higher than the initial stiffness of Frame01 (quasi-static) due to dynamic effects. In the Frame01 quasi-static test, the failure progression occurred within the vicinity of indentation. Also in Frame01, there were competing failure mechanisms between penetration of the C-frame through the stringers and cracking of the C-frames where the stringers contacted the C-frames. In the quasi-static test, there was local damage and deformation (equating to more energy released and more intermediate damage) at the stringer-frame contact site. The quasi-static test allowed for sufficient time for the load to redistribute through redundant load paths, which could lead to higher overall loads.

When Frame03 was impacted dynamically, the frames experienced a combined torsion+shear+bending failure close to the boundary conditions, and away from the impact area. This suggests the load transfer through the frames into the boundaries, and the resulting response leading to failure of the frame, is load-rate dependent. In both dynamic and quasi-static cases the stringer-frame interaction played a critical role in the damage evolution. It should be noted that for this type of impact, not only should the impact site be inspected but also the surrounding areas (i.e., where the frames join to other structures, such as the connection to the cargo or passenger floor).

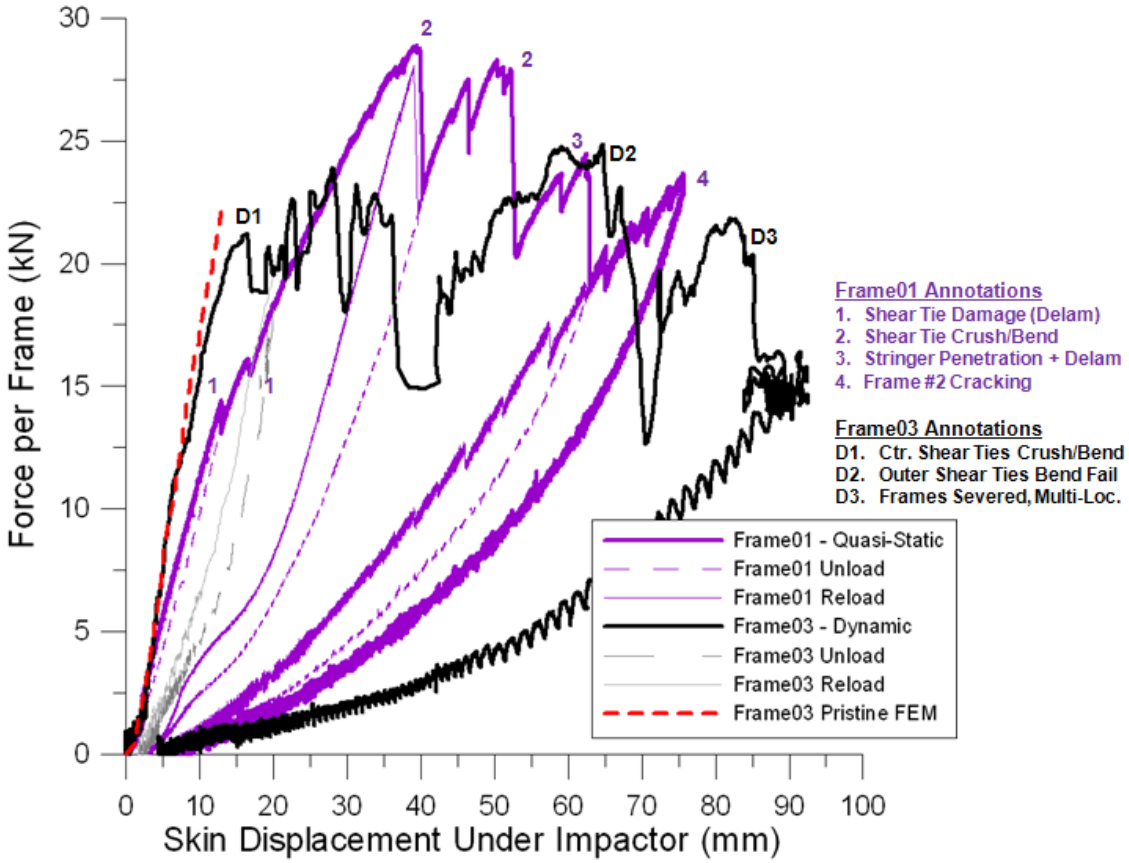

Figure 16. Force per Frame Comparison for Quasi-Static and Dynamic Impact Events

2.4.3 FrameXX Specimens – Analysis

A methodology to analyze the High Energy, Wide Area, Blunt Impact phenomenon is currently under development. Specifically, a deeper understanding is sought on how the key structural parameters of the panel effect the damage initiation and evolution upon impact, which will be reflected in the finite element modeling approach. A script based model build approach is in progress that will automatically generate finite element models consistently and efficiently, making use of python script executed in ABAQUS. The script will include Hashin-Rotem failure parameters for failure within the composite

laminate and cohesive surfaces to model delamination between the stringers and skin. A force-displacement history (per frame) for a preliminary model created with the script shows good correlation to the experimental data during the initial elastic up-loading, as shown in Figure 16. The models, upon being validated by experimental data, will help gain further insight into the experiments and extend the experimental results to more general cases – e.g., different panel geometry and boundary conditions.

2.5 GSE Blunt Impact Conclusions

The following set of conclusions can be drawn based on the low velocity blunt impact activities.

- **Experiments – StringerXX Specimens**
    - Dynamic localization effects are observed when a panel is impacted on the skin between stringers, where damage was found to be localized for dynamic impact (Stringer05), and more widespread for quasi-static indentation (Stringer02).
    - Dynamic impacts (in the order of 0.5 m/sec) with the 76.2 mm wide OEM bumper produced externally visible cracks on the panel surface.
- **Experiments – FrameXX Specimens**
    - Significant damage requires high forces – e.g., ~70 kN (15,700 lbf) on impact across three frames. For this type of event there will be loud noises and a global response in the aircraft (entire aircraft will move).

- Contact between frames and stringers plays a major role by promoting rotation of the C-frames and leading to damage further away from the impact site for dynamic tests.
- No exterior visibility (cracks) develops for long bumper contact on skin between stringers, loaded across frames.

- **Analysis**
  - Cohesive surfaces and the Hashin-Rotem failure criteria in the ABAQUS can be used to properly predict the formation of delaminations and cracks.
  - For the FrameXX specimens, the contact definition between the stringers and frames plays an important role in the damage evolution of the frames. It is especially important to capture the correct rotation of the C-frame.
  - Approximation of the D-shaped, OEM bumper with a flat pad (i.e., a pre-collapsed bumper) in the FE simulation is validated as they produce the same uploading curve. This allows for a computationally less expensive bumper model and avoids numerical instability issues of the collapsing bumper.

3.0 High Velocity Ice Impact Damage to Composites

3.1 Background and Motivation

The continued and expanding use of composites as load carrying aircraft structures that are exposed to the natural environment means that they are subject to potentially damaging impacts from a variety of sources, a major one

being hail ice. Structures that fall into this category include aircraft radomes, fuselages, wings, empennage, and nacelles. Hail impact events citing hailstones ranging from golf ball to tennis ball size are not uncommon. This occurs both at the terminal velocity of hail falling to the ground (approximately 30 m/s) and at the in-flight speeds of an aircraft (around 200 to 250 m/s).

Additionally, hail will often impact the structure at different glancing angles, both while in flight and on ground, due to the varying geometry of the aircraft. These angled impacts may cause damage which differs from that of normal impacts due to the fact that glancing impacts produce a sliding contact condition acting over a moving area. The damage modes and size of angled impacts compared to normal impact should therefore be clearly understood. An overall understanding of what velocities and trajectories of ice causes damage is important for establishing the damage resistance to the ice impact threat, and for aiding in developing metrics for inspection. Furthermore, the ability for prediction of non-visible internal damage, such as delamination, due to hail ice impact is critical in the decision for further inspection of aircraft parts following the occurrence of hail impact event.

3.2. Summary of Previous Results

A procedure was developed to obtain the high velocity impact failure threshold energy (FTE) of panels. This included the use of non destructive evaluation to find damage and a logistic regression to identify FTE value. The failure thresholds of nine combinations of panel thicknesses and simulated hail ice (SHI) diameters were experimentally determined. Previous results also

determined that the failure threshold was dependent primarily on the panel thickness and SHI diameter but not strongly on material form (tape versus woven). This conclusion was achieved through a comparison of the current data on tape material with previous FTE measurements on fabrics. Additionally, a finite element analysis (FEA) model was developed. The FEA results demonstrated the experimentally-measured and FEA-predicted damage threshold velocities to be consistent with each other. This provided confidence that the methodology used for the numerical simulations was valid, especially since no "tuning" of FEA material parameters was done to achieve correlation.

3.3 Recent Results

Recent progress has been achieved in modeling and damage prediction focused aspects of ice impact onto composites. These are described in the following subsections.

3.3.1 Solid Cohesive Modeling and Damage Prediction Results

The impact experiments identified the FTE and associated failure threshold velocity (FTV) for each combination of panel thickness and SHI diameter. The setup and results were presented in the 2011 report and can be found in literature [4]. Independent of the experimental values, a series of FEA models were created and exercised. The models were defined to represent the experimental setup. Figure 17 shows an example of the 8 ply panel being impacted by a 50.8 mm SHI (simulated hail ice, referring to lab-cast spheres as opposed to naturally-occurring hailstones). The composite panel was modeled

ply-by-ply with an individual layer of solid continuum elements representing each ply. The plies are defined as an orthotropic material with principle material directions oriented based on ply angle. These properties are given in Table 3. Cohesive elements were placed between each ply layer of the panel in order to predict delamination. The elements are defined with a traction-separation law having a damage initiation based on quadratic stress criteria, involving interlaminar stresses and damage evolution based on mixed mode energy using a power law. Fracture energy parameters are used for damage propagation. The density and stiffness parameters were calculated in accordance with ABAQUS user manual recommendations based on the solid mesh defined adjacent to the cohesive elements.

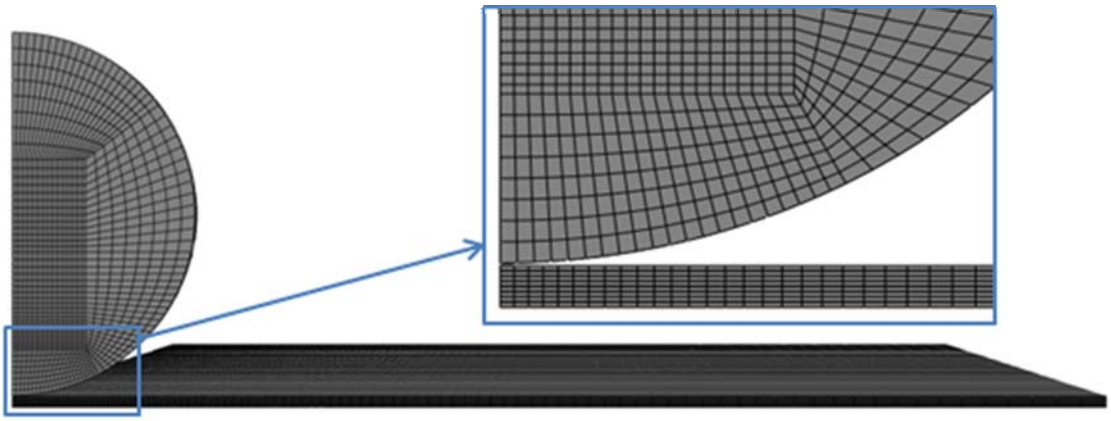

Figure 17. Quarter Symmetric Mesh of 50.8 mm SHI Impacting 8 Ply Composite Panel

Table 3: FEA Material Properties

Orthotropic Composite Lamina	
Quantity	**Value**
Young's Modulus: E_1	160.08 GPa
Young's Modulus: E_2	8.97 GPa
Young's Modulus: E_3	8.97 GPa
Poisson's Ratio: v_{12}	0.28
Poisson's Ratio: v_{13}	0.28
Poisson's Ratio: v_{23}	0.36
Shear Modulus: G_{12}	6.21 GPa
Shear Modulus: G_{13}	6.21 GPa
Shear Modulus: G_{23}	3.45 GPa
Density: ρ	2,700 kg/ m^3
Ply Thickness: t	0.195 mm

Cohesive Elements	
Quantity	**Value**
Stiffness: K_{33}	461,500 GPa
Stiffness: K_{13}	461,500 GPa
Stiffness: K_{23}	461,500 GPa
Strength: S_{33}	50 MPa
Strength: S_{13}	115 MPa
Strength: S_{23}	115 MPa
Fracture Toughness: G_{IC}	710 N/m
Fracture Toughness: G_{IIC}	2,200 N/m
Fracture Toughness: G_{IIIC}	1,700 N/m
Density: ρ	0.05265 kg/ m^3

The model was used to conduct "numerical experiments" to predict the FTV. To do this, the model was first run at a velocity near the expected FTV. If no damage was indicated by the separation of the cohesive elements then the velocity was increased. If damage was predicted, then the velocity was decreased. This method was repeated until bounding velocities within a 5 m/s range were determined. These bounding velocities were then averaged to obtain the FTV FEA values shown in Table 4. The FEA predictions are consistent with experimental results, and always predict slightly low FTV values. Note that for the 24 ply panel impacted by the 38.1 mm SHI, a numerical instability was present in the FEA results due to the high velocity, and thus this case is still under investigation.

Table 4. Experimental and FEA Based FTV results

Panel Type (Thickness)	SHI Diameter (mm)	FTV Experimental (m/s)	FTV FEA (m/s)	Percentage Difference
8 ply (1.59 mm)	38.1	115	97.5	15
	50.8	91	67.5	26
	61.0	65	47.5	27
16 ply (3.11 mm)	38.1	154	147.5	4
	50.8	121	107.5	9
	61.0	96	82.5	14
24 ply (4.66 mm)	38.1	178	N/A*	--
	50.8	154	152.5	1
	61.0	127	117.5	7

*Numerical singularity present in FEA model

In addition to the FTV, the FEA predicted the contact force histories of each impact. Figures 18 to 20 show the 8, 16, and 24 ply panel impact force histories for the impact velocities that bound the FTV within the 5 m/s range. The star marker shown on the upper bound plots indicate when the first cohesive element fails. Of particular interest was the (non-intuitive) observation that the peak force of these damaging impacts, referred to as the critical force, was essentially the same for each panel thickness regardless of SHI diameter and velocity. In order to achieve the same force level, a smaller diameter SHI must impact the panel at higher velocity. Increasing panel thickness required higher critical force to initiate damage, which is reflected in the Table 5 summary showing higher velocity needed for a given SHI diameter to initiate damage in thicker panels.

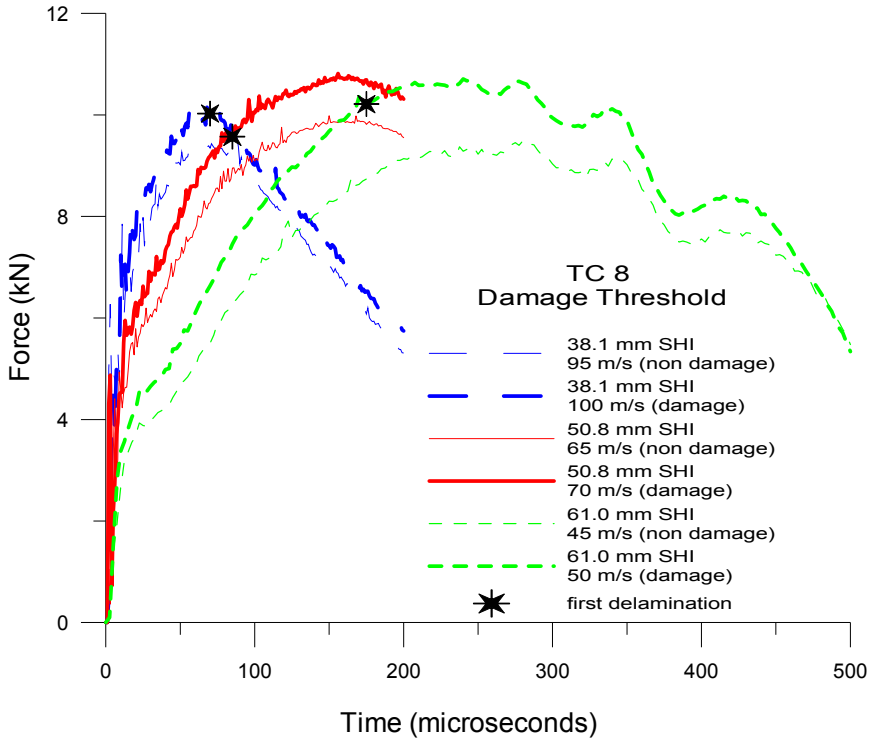

Figure 18. Force Histories for the Bounding Velocities of 8 ply Panels

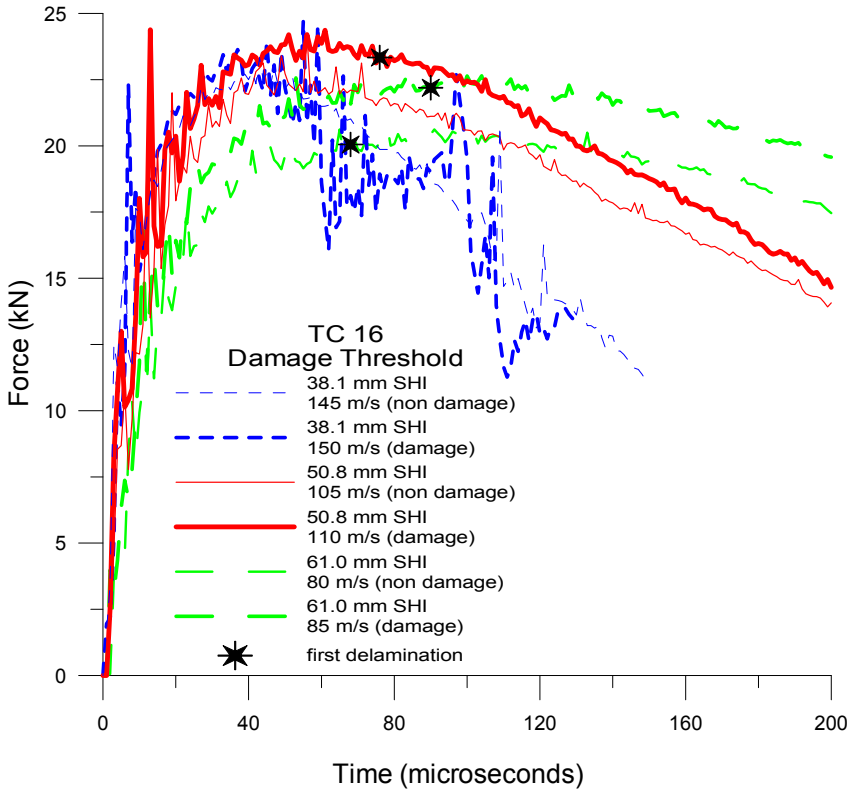

Figure 19. Force Histories for the Bounding Velocities of 16 ply Panels

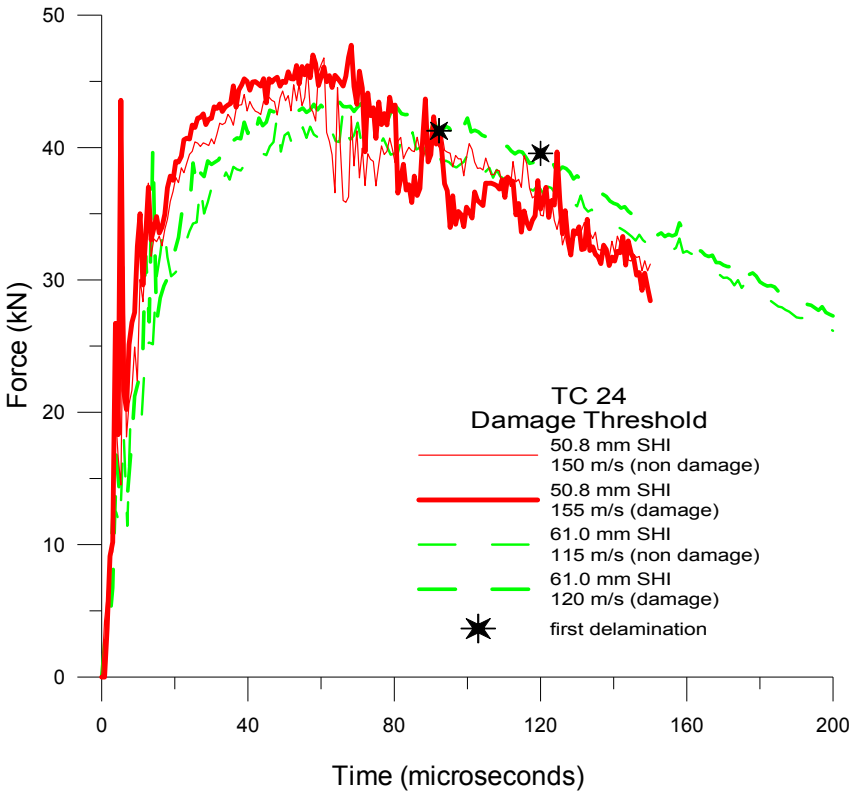

Figure 20. Force Histories for the Bounding Velocities of 24 ply Panels

Table 5. FEA Based FTV and Peak Force Results

Panel Type (Thickness)	SHI Diameter (mm)	FTV FEA (m/s)	Critical Peak Force (kN)
8 ply (1.59 mm)	38.1	97.5	9.7
	50.8	67.5	10.2
	61.0	47.5	9.9
16 ply (3.11 mm)	38.1	147.5	22.2
	50.8	107.5	23.2
	61.0	82.5	21.4
24 ply (4.66 mm)	38.1	N/A*	--
	50.8	152.5	44.5
	61.0	117.5	42.0

3.3.2 Shell Modeling and Force Scaling Results

A force criterion allowed for the simplification of the panel portion of the FEA, from a solid model with cohesive elements to shell elements. The computational cost was dramatically reduced by representing the through-thickness direction of the panel with a single layered shell element. The composite lay-up and properties were maintained by use of ABAQUS shell composite command. Figure 21 is a plot of the force histories for simulated hail ice impacts onto solid and shell composite panels at the experimentally determined critical velocities. The force histories of the shell models match the histories previously predicted by solid element models. Since force is the key parameter for damage prediction, i.e., via the critical threshold force, shell models can be used for analyzing larger complex structures, with a reliance on critical force as a failure criterion for predicting the onset of damage.

Using the shell models a parametric study was completed focusing on the contact force generated for a verification of experimental parameters, most critically, the velocity. Specifically: three SHI diameters, 38.1, 50.8, and 61.0 mm, and four target types, 8 ply, 16 ply, 24 ply, and rigid panels were examined. Each of the 12 combinations were analyzed for three velocities: 80, 100, and 120 m/s. As expected, the peak force was higher for stiffer targets, with maximum possible force developed in association with the rigid limit (for a given ice diameter and velocity combination). The peak forces from the study are summarized in Table 6.

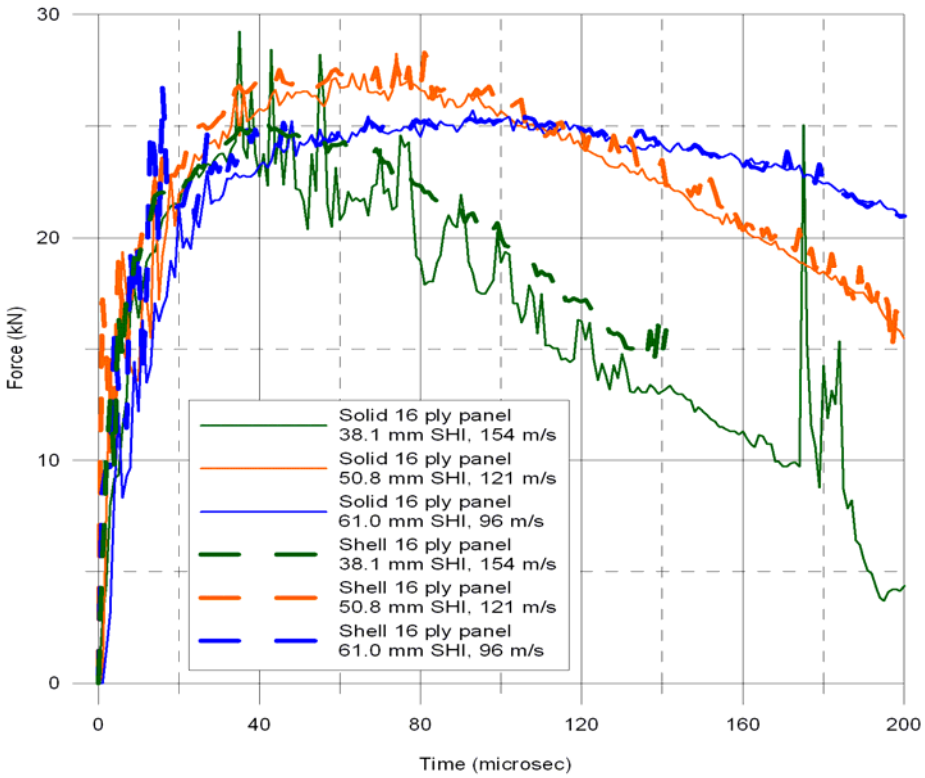

Figure 21. Force Histories for Shell and Solid 16 ply Panels

Table 6. Study Peak Force Results

Panel Type (Thickness)	SHI Diameter (mm)	Peak Force Critical* (kN)	Peak Force 80 m/s (kN)	Peak Force 100 m/s (kN)	Peak Force 120 m/s (kN)
8 ply (1.59 mm)	38.1	12.3	7.6	10.2	12.9
	50.8	14.3	12.2	15.8	20.6
	61.0	14.7	16.8	22.5	28.0
16 ply (3.11 mm)	38.1	24.3	11.1	14.2	18.0
	50.8	28.2	15.6	21.4	27.0
	61.0	25.7	20.2	27.3	35.4
24 ply (4.66 mm)	38.1	33.9	13.3	17.1	21.2
	50.8	44.3	19.9	26.5	33.2
	61.0	47.9	26.5	34.1	43.8
Rigid	38.1	n/a	16.8	21.9	26.9
	50.8	n/a	30.4	38.6	47.6
	61.0	n/a	44.3	55.8	67.9

*Note: found for simulations run at FTV for each case – see Table 4

3.3.3 Glancing Impact

The objectives of this glancing ice impact activity were to: (i) determine the FTE of composite panels subject to glancing impacts at angles ranging from 20 to 40 degrees, (ii) gain insight into the onset of damage via dynamic finite element analysis of glancing impacts, and (iii) compare the visual detectability (dent depth) of impacts onto composite panels relative to baseline 2024-T4 aluminum alloy panels of equivalent in-plane stiffness.

A series of high velocity impact experiment were conducted with SHI of 50.8 and 61.0 mm diameter. The SHI was projected at speeds ranging from 70 to 245 m/s onto 8 and 16 ply carbon/epoxy panels (Toray T800/3900-2 unidirectional tape) having quasi-isotropic layup. The panels were impacted at glancing angles between 20 to 40 degrees, where 90 degrees indicates normal impact. As expected, higher velocities are required for lower glancing angles in order to initiate damage. This velocity associated with the damage onset is referred to as the failure threshold velocity (FTV). Figures 22 and 23 plot the experimentally measured FTV for the 8 and 16 ply panels. Included in these plots are trends based on the scaling of the FTV_{90} (the FTV associated with normal impacts). These trigonometric scaling curves predict the higher values of FTV for lower glancing angle based on equating either the normal component of the incoming velocity, or the normal component of the incoming kinetic energy, to FTV_{90} (or FTE_{90}). As shown in Figures 22 and 23, the two trends define an upper

and lower bound within which the actual FTV exists, over the range of glancing angles studied.

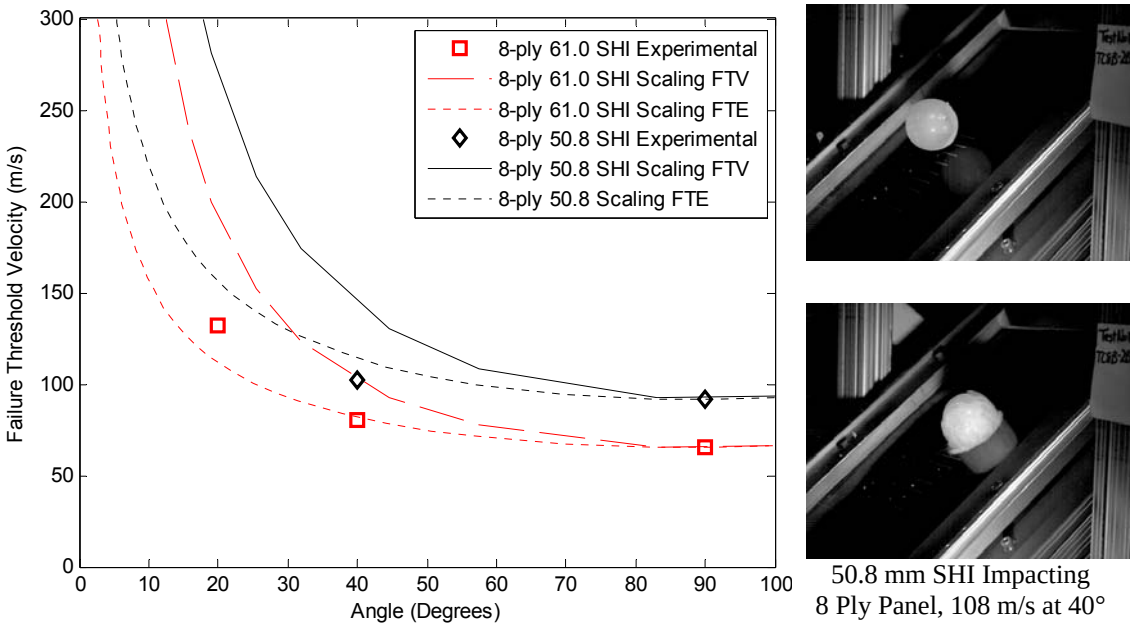

50.8 mm SHI Impacting 8 Ply Panel, 108 m/s at 40°

Figure 22. Experimental FTV of 8-Ply Panels with Trigonometric Scaling of Normal FTV and FTE

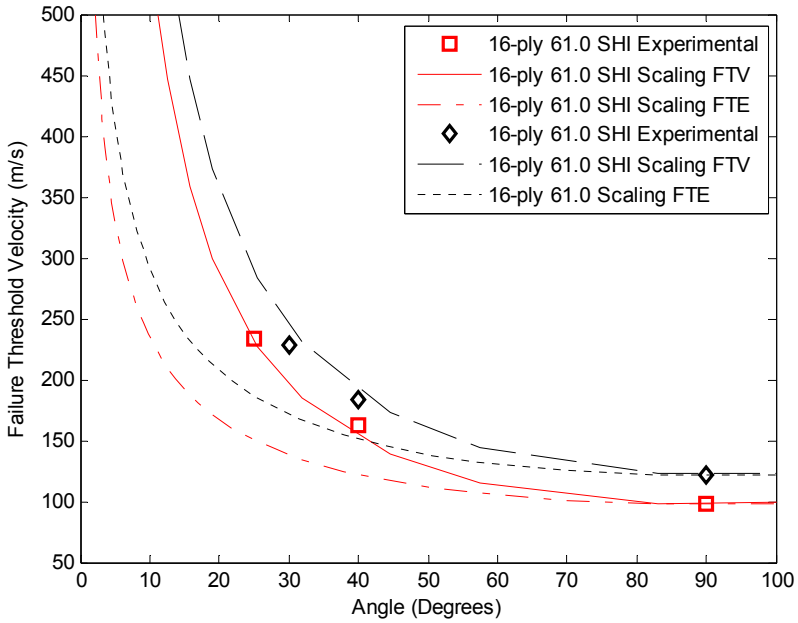

Figure 23. Experimental FTV of 16-Ply Panels with Trigonometric Scaling of Normal FTV and FTE

Explicit dynamic Finite Element Analysis (FEA) of the glancing impacts has found that the same level of peak interlaminar shear stress develops in the panel at FTV (experimental value used as input to the simulations) regardless of glancing angle, diameter, and panel thickness (see two conditions plotted in Figure 24 showing peak interlaminar shear ~ 110 MPa). Thus peak interlaminar shear stress is considered to be a simple criterion by which the onset of delamination can be estimated using numerical models. Maximum interlaminar shear stress is known to be a key parameter associated with delamination onset during a localized impact event.

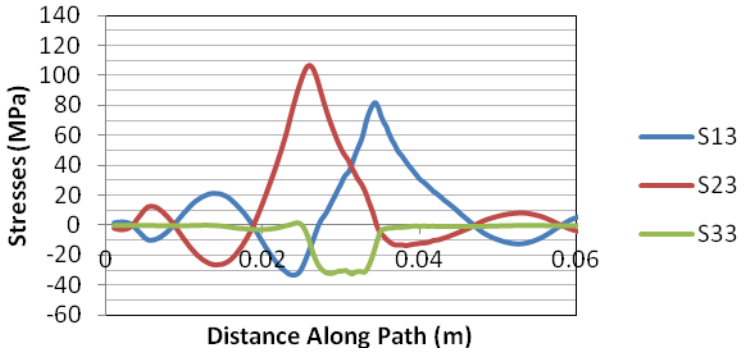

(a) Stresses for 20 Degree Glancing Angle, 61.0 mm SHI, 8-Ply Panel, FTV = 132 m/s

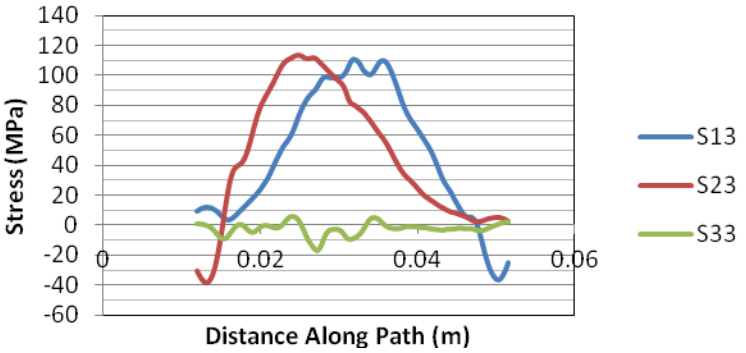

(b) Stresses for 30 Degree Glancing Angle, 50.8 mm SHI, 16-Ply Panel, FTV = 229 m/s

Figure 24. FEA Predicted Interlaminar Stress Components for SHI Impact Corresponding to FTV

Finally, dent depth measurements comparing dents in 8 ply composite panels to the dents in 1.6 mm aluminum are plotted in Figure 25. Similar results exist for the 16 ply panels compared with 3.2 mm thick aluminum. The aluminum can be seen to develop 1 to 2 orders of magnitude deeper dents, in comparison to the composite, over the same energy level range. The composite panels tended to exhibit nearly unobservable dent depths even when significant delamination occurred. Therefore, reliance on visual observation to detect the presence of hail ice impact damage is not a reliable way to find hail ice impact damage.

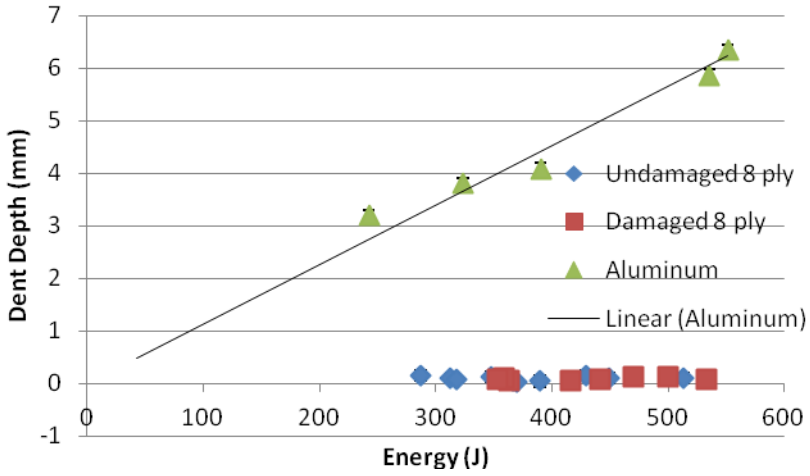

Figure 25. Maximum Dent Depths vs. Impact Energy of Projectile at 40 Degrees; Al Panel 1.6 mm Thickness

3.3.4 Impact on Stringer-Stiffened Panels

Studies of SHI impacts on stiffened carbon/epoxy panels are being carried out to determine how damage initiation is affected by impact location with respect to internal stiffeners. The stiffened panels were made of Toray T800/3900-2

unidirectional carbon/epoxy, with a 16 ply quasi-isotropic skin and hat-shaped stringers stiffeners. SHI of 61.0 mm diameter were impacted onto the stiffened panel at normal incidence angle using a gas gun. The FTE of 305 x 305 mm flat panels of 16 ply quasi-isotropic layup impacted by 61.0 mm ice was used as a baseline energy value [4]. This baseline value of 489 J is multiplied by a factor ranging between 0.25-2.0 to define a "knockdown" factor which describes how the FTE is affected by various impact locations on the panel. These impact locations are: middle of stringer, stringer flange, on skin spanning the middle of a bay, on shear ties, etc., as described in Figure 26. Preliminary results summarizing the lowest energy level at which damage was found to occur can be found in Table 7. The current study involves stringers with 38 mm tapered flanges. The varying types of damage and damage levels will be observed. Future plans include impacting and observing panels with stringers that are not tapered (i.e., truncated at 38 mm). A comparison of the different types of stringers will be done.

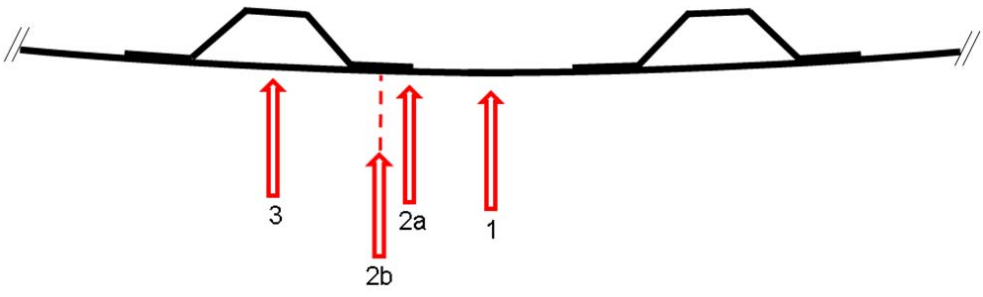

Figure 26: Types of Impact Locations. (1) Middle of the Bay,(2a-2c) Stringer Flange, (3) Middle of Stringer, and (4) on Sheartie (Not Pictured).

Table 7: Preliminary Results on Knockdown Factor for Impact Locations

Impact Location	Knockdown Factor
I1 – Middle of bay	1.1
I2a – End of stringer Flange	0.3
I2b- Middle of stringer Flange	0.3
I3 – Middle of Stringer	NA
I4 – Directly over Shear Tie	1.3

3.4 Discussion

The peak contact force values associated with the critical velocity were found through FEA models. Such contact force data are not readily measurable by experiments involving high velocity projectiles that crush upon impact. The critical force values were unique for each panel thickness tested, but did not change with the variation of SHI diameter. When plotted versus panel thickness, the critical force was observed to follow a linear trend. This useful result is material and layup dependent, however, and thus in an effort to generalize the results, an effective bending stiffness, D* (developed by Robin Olsson [5]), was used instead to describe the panel characteristics. This is given in Eq. (1).

$$D^* = \left[D_{11}\ D_{22}\ \frac{(\eta+1)}{2}\right] \quad (1)$$

where

$$\eta = \left[\frac{D_{12}+2\ D_{66}}{(D_{11}D_{22})^{1/2}}\right] \quad (2)$$

The cube root of D* has the same dimensional form as the panel thickness. Therefore, the critical force is found to relate linearly to $(D^*)^{1/3}$ as shown in Figure 27. If the peak force of an impact is known, conceivably from a

less computationally expensive model (e.g., involving shell elements), this plot can be used to predict if damage has occurred in a panel by SHI impact.

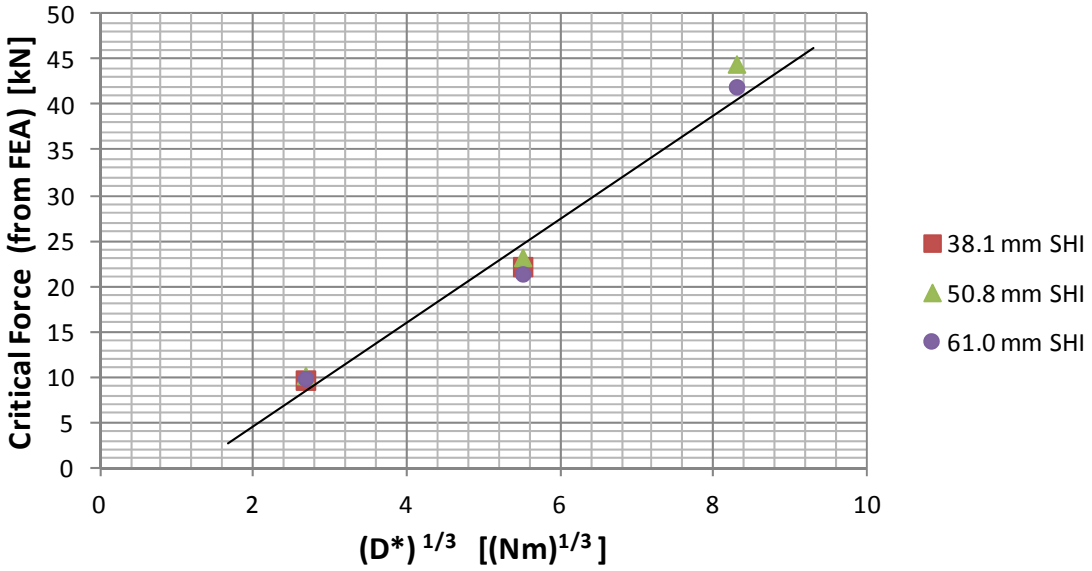

Figure 27. Critical Force versus Effective Bending Stiffness to One-third Power

Further data manipulation allows development of Figure 28, which shows panel information on the x-axis (specifically the cube root of the effective bending stiffness) and projectile information on the y-axis (where *d* is the diameter and V_{FTE} is the failure threshold velocity of the SHI corresponding to FTE). Ice diameter and velocity are quantities that define the impact threat and are readily known for an impact event. These are often specified as requirements against which structures must show resistance to impact damage, and thus Figure 28 provides a quick damage prediction capability based on three known key parameters: ice diameter, velocity, and panel effective bending stiffness (embodies thickness + layup information). Additionally, this plot can be used as a tool for establishing the minimum diameter for which an impacted aircraft skin

would require inspection following a hailstorm. The applicability of these results extends generally to toughened carbon/epoxy composite materials having a similar level of interlaminar strength (see Table 3), since the interlaminar strengths are the key material properties used by the FEA models to trigger onset of failure in the cohesive elements.

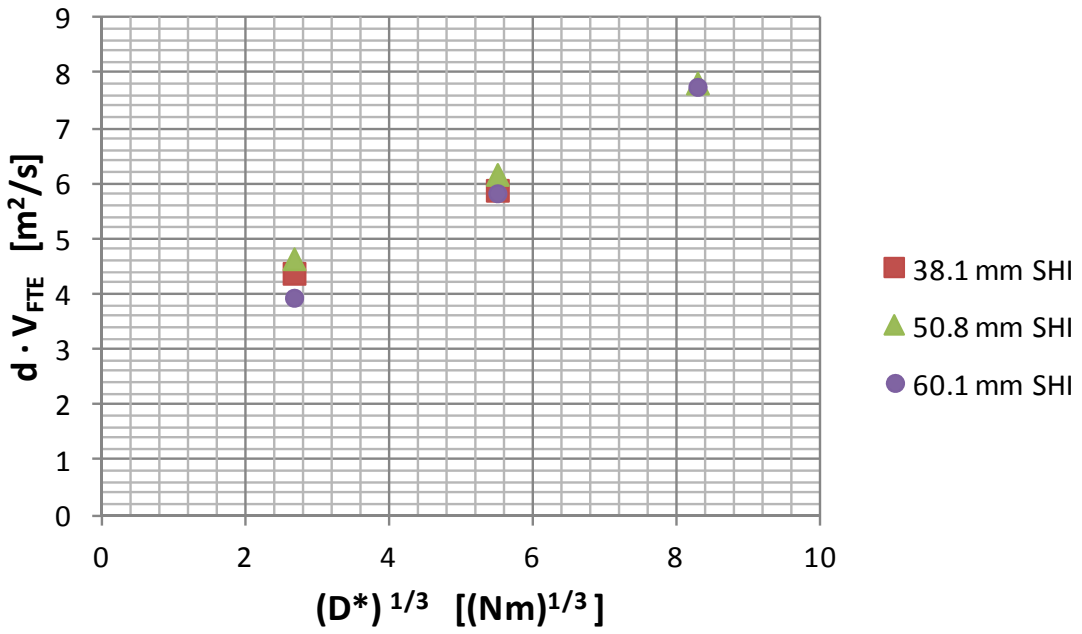

Figure 28. SHI Diameter times Critical Velocity versus Effective Bending Stiffness to One-third Power

In addition to damage prediction capabilities, the development of a force scaling tool was investigated. Experimental determination of peak force for SHI impact onto flexible targets is not possible. Therefore, a link between the rigid and flexible target impacts was established through the interpretation of the results from the FEA parametric study. The peak force values in Table 6 are found to increase linearly with both velocity and SHI diameter. Figure 29 summarizes the data of Table 6, collapsing all velocities, ice diameters and panel

thicknesses into a single relationship between two parameters. The first parameter is the peak force ratio (PFR) which is the peak force of an impact onto a flexible target normalized by the peak force for that same impact (i.e., same SHI diameter and velocity) onto a rigid target. The second parameter is the ratio of panel thickness, H, divided by the SHI diameter, D.

A single linear trend is thus identified which can be used to determine the peak force of SHI impact onto a flexible target as long as the SHI diameter, the panel thickness, and the peak force for rigid target impact are known. Once a peak force prediction onto a flexible target has been established, the value can be compared to the critical force value established by the finite element force results corresponding to the experimentally determined critical cases (see Table 4).

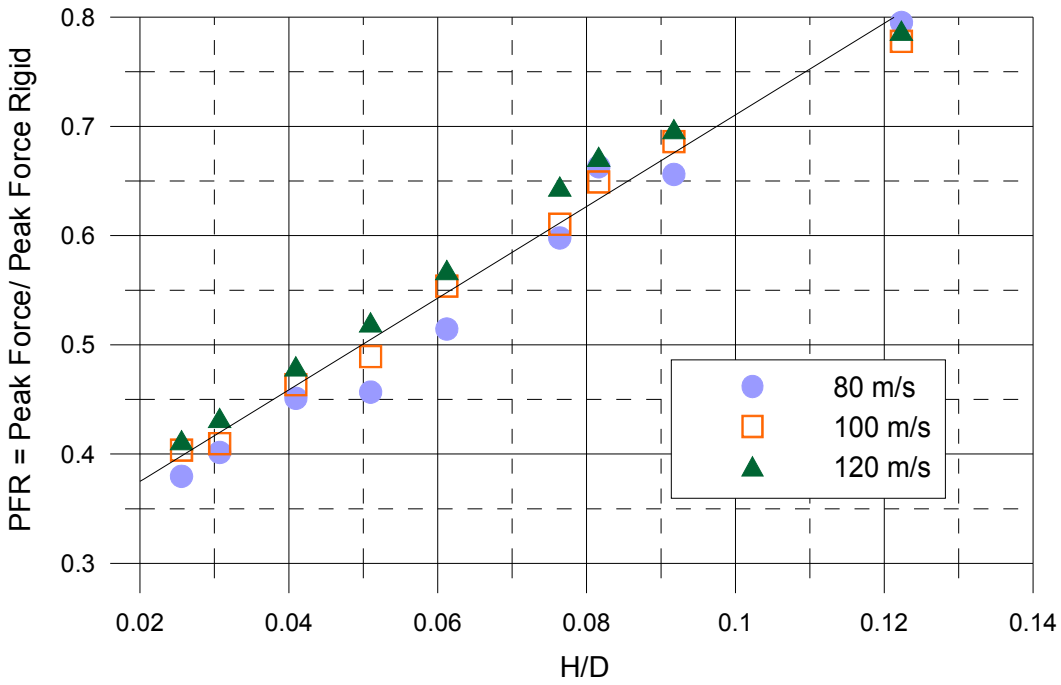

Figure 29. Peak Force Ratio (PFR) Linking Flexible and Rigid Target Impact

3.5 Ice Impact Conclusions

- The FEA models including cohesive elements are considered to be predictive, since the panel material properties are all based upon values found in the literature for this material system, and no parameters were tuned to match the experimental results. The results of this model are generated independently and found to be consistent with experimental results.
- The models have been used to reveal that a panel of a specified thickness and material has a critical force level at which damage onset will occur. This critical force is independent of the SHI projectile diameter. Such an observation provides the basis for establishing a threshold force failure criterion that would define the initiation of damage in a manner that is independent of the projectile diameter.
- A linear relationship was established between key parameters, which include the ice diameter and velocity (defines impact threat) and the panel effective bending stiffness. This linear relationship can be used as a design-oriented tool for skin sizing, establishing minimum gage thickness based on hail impact requirements, or threat assessment of an already established laminate design.
- Shell model force outputs are equivalent to the more expensive solid + cohesive elements model. Using a force based criteria for predicting damage initiation could conceivably be lower cost (computationally) by not

requiring the use of expensive cohesive elements and multiple layers of solid elements.

- The experimental results show a linear relationship between peak force generated for rigid target impact and kinetic energy. The analytical results produce trends of peak force for SHI impacts onto flexible composite panels over a range of velocities, as well as the critical force values associated with the experimentally determined threshold impact energies. A unified linear scaling relationship was then determined which allows the prediction of peak force on composite panels based on the directly measured peak force data from rigid (instrumented) target impacts. This scaling is found to depend only on the panel thickness to SHI diameter ratio, H/D.

4.0 Low Velocity Impact by Large Radius Metal Tips

4.1 Background and Motivation

Low velocity impact tests with large radius metal tips were conducted to determine the relationship between the damage thresholds and impact tip radius for different thicknesses of T800/3900-2 graphite/epoxy composite panels, and to investigate the type of damage caused by these impacts. Impact tests have been performed on graphite/epoxy panels 8, 16, and 24 plies thick with impact tip radii of 12.7, 25.4, and 50.8 mm.

Because of an increased demand for composite materials in aviation and the vulnerability of these materials to impact damage, it is important to have a

greater understanding of the material behavior subject to impact damage. Aircraft are often exposed to a variety impact threats such as runway debris, tool drops, and collisions with ground equipment. These experiments seek to establish a more comprehensive description of composite material behavior subject to blunt impact loads with hard tips (i.e., non-deforming).

4.2 Summary of Previous Results

Whisler has previously investigated low velocity impact damage with relationship to the impact tip radius on woven glass/epoxy panels [6]. His work has found that while the impact force was not affected by the tip radius for a given energy level, the energy required to initiate damage was. The larger impact tip radii created a larger contact area during the impact, which reduced the average contact pressure on the panel. Because of this, the failure threshold energy increased with increasing impact tip radius, so a blunter impact tip required more energy to initiate damage than a sharper tip.

4.3 Recent Results

In the current investigation, tests to date have found that the failure threshold energy increases with panel thickness and impact tip radius. These tests have established preliminary values for the failure thresholds of each test parameter. Table 8 shows the failure threshold energies for each panel thickness and impact tip radius established from the test data collected so far.

Table 8. Failure Thresholds Energies

Panel	12.7 mm	25.4mm	50.8mm
8 ply	10 J	9 J	20 J
16 ply	16 J	20 J	40 J
24 ply	20 J	34 J	43 J

The primary forms of damage from impacts on the panels are surface denting and delamination. Higher energy impacts can also result in back face fiber breakage. Figure 30 shows a microphotograph of the cross section of a damaged 16 ply panel, impacted by a 12.7 mm radius tip. In this figure all three forms of damage are present. Although the delamination in the image is not obvious, it is apparent with close (destructive) inspection under a microscope.

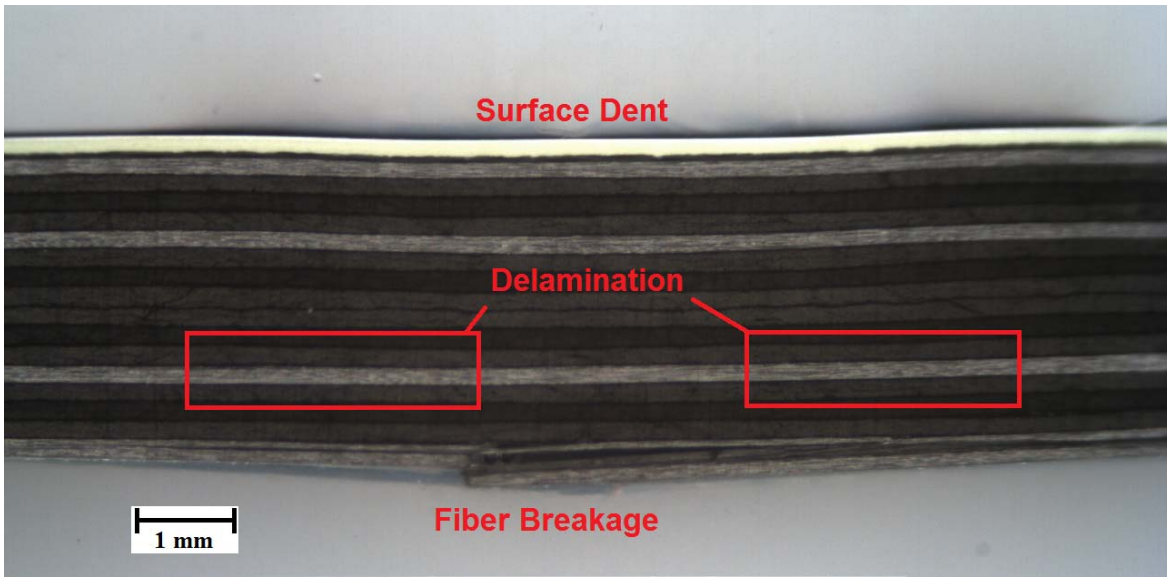

Figure 30. Microphotograph of Damaged 16 Ply Panel Created by 12.7 mm Radius Tip Impact

A notable result has been the depth of the surface dent created by the impact. Tests have shown that the dent depths are deeper for smaller impact tips and higher impact energy, but are not necessarily indicators of internal damage. With the 50.8 mm radius impact tip, internal damage can be caused without any measurable or visible surface dent, but some tests with the 12.7 mm radius tip have caused significant surface dents with no internal damage. Another notable result regarding the surface dents is that the depth of the dent can decrease over time, i.e., relax. To record this, the surface dents were recorded immediately after impact test as well as one day following the impact. Figure 31 shows the initial and relaxed dent depths for tests with the 12.7 and 50.8 mm radius impact tips, as well as whether internal damage was created. The initial dents created by the 12.7 mm radius tip relaxed to some measurable level, while the 50.8 mm tip relaxed to either nothing or barely measurable level (0.02 mm).

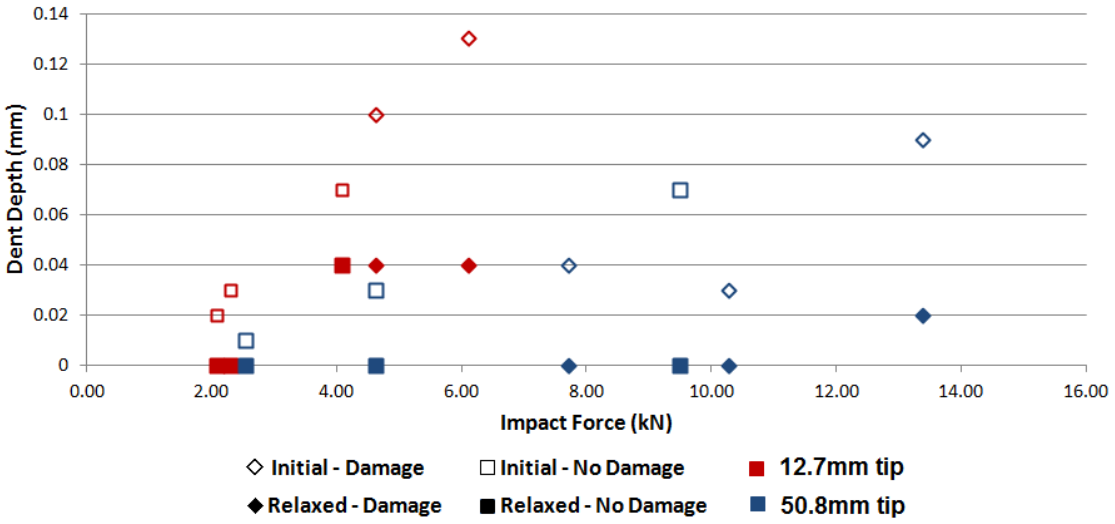

Figure 31. Initial and Relaxed Dent Depths for 12.7 and 50.8 mm Radius Impact Tips

4.4 Discussion

The increasing failure threshold energy with panel thickness and impactor radius is consistent with previous work on glass/epoxy panels. This means that the failure threshold is dependent on the average contact pressure and not just the total force from the impact. The surface dents caused by the impacts are a form of visible damage, but do not necessarily indicate internal damage. These surface dents have been observed to relax and become less visible over time. This emphasizes the importance of reporting possible impact damage as it occurs. If an impact event goes unreported then the damage is even more likely to be missed during later inspections.

4.5 Low Velocity Large Radius Metal Tip Impact Conclusions

- The failure thresholds increase with both panel thickness and tip radius.
- The primary forms of damage are surface denting and delamination, followed by back wall fiber breakage with increasing energy.
- Impacts often create a visible surface dent which are more pronounced with the smaller impact tips than the blunt ones.
- Dent formation does not necessarily indicate internal damage. Internal damage can be present without a surface dent and surface dents can be present without internal damage.
- Dents measured immediately after the impact event will be deeper than when measured at another point in the future. The dent relaxes, decreasing in depth as well as visibility.

5.0 Benefits to Aviation

The UCSD focused research on impacts threats which can produce non-visible damage have several key benefits to aviation. These are summarized below:

5.1 GSE Blunt Impact

- Understanding of damage produced from wide-area GSE impact events through experimental data and finite element analysis. This provides awareness of the blunt impact phenomena and an anticipation of the internal failure modes, as well as the extent of this damage and what energy levels are needed to produce various damage levels.
- Establish experimental methods – full vs. substructure and importance of correct boundary condition representation, how to account for dynamic effects.
- Establish analytical capability to predict blunt impact damage by simple models based on energy balance, force failure threshold (estimate onset of damage), and vehicle mass and speed at time of impact. Also develop a methodology to build nonlinear FEA models that include damage evolution.
- Identify how to detect and monitor the occurrence of damaging events. Particularly what inspection techniques and sensor technology could be used.

5.2 Ice Impact

- Estimation of the damage threshold of composite structures based on the analytical results. Allows for efficient design, namely skin sizing, of composite structures to be resistant to impacts at specific hail conditions.
- Models allow prediction of damage onset (i.e., FTE) which can decrease the cost of aircraft development programs by reducing the amount of testing required.
- An understanding of what ice conditions (size, velocity, relative location on aircraft, etc.) cause damage on an aircraft is important to defining what conditions require machine-assisted inspection (e.g., ultrasonic scan).

5.3 Large Radius Metal Tips

- Deeper understanding of material behavior subject to impacts, particularly how increased radius affects damage formation and visual detectability.
    - Establish correlation between the onset of damage and the radius of the impactor.
    - Determine the relationship between visible damage and internal damage.
- Material level test described by failure threshold force results are applicable to other conditions and specimen configurations.

6.0 Future Work and Follow-On Activity

The project activities summarized herein are ongoing. Future planned and recommended activities are described below.

GSE Blunt Impact

- Complete *dynamic* blunt impact test on Phase II large 5-frame specimen (Frame04)
    - dynamic impact vs quasi-static indentation – rate, scaling, and BC effects
- Continued developments to establish high fidelity FEA modeling capability
    - damage initiation, progressive failure process, damage extent, energy absorption
        - correlation to large panel test results – use direct material properties (no "tuning")
        - define visibility metrics compatible with FEA
    - cohesive surfaces implementation into shell-based models to represent delamination
- Develop and refine reduced order models
    - estimate damage onset for wide parameter range: GSE mass, velocity, impact location
    - relate test results to GSE field operations
- New investigations needed (experimental + analytical):
    - glancing impacts effects
        - define scaling relationships via momentum and angle
        - moving contact area – e.g., pushing across multiple stringers
    - boundary condition and dynamic localization effects on larger sized specimen – ¼ or ½ barrel with floor structures and joints

    - metal fuselage for metal baseline compare – particularly visibility aspects
    - other primary structure types – e.g., wing, tail
- Education/Training: dissemination of results, workshops.

Ice Impact

- Hail ice damage resistance and morphology for panels/structures of sandwich construction.
- Investigate effect of multi-hit and impact adjacency.
- Investigate stiffened skin impact effects and establish prediction capability – both empirically-based and FEA simulation.
- Education/Training: dissemination of results, workshops.

Large Radius Metal Tips

- Test with larger radius tips (76.2 mm planned) to get more detailed picture of the effect the impactor radius has on the damage thresholds.
- Perform additional tests to refine the failure threshold data. With a more precise failure threshold the effect of the tip radius will be better defined.
- Investigate dent relaxation by recording depth versus time for tests that cause significant dents. This gives insight into visually identifiable damage in the field.
- Compression after impact testing - what is the residual strength of panels that have experienced the types of damage that have been observed?

- Use photogrammetry to further characterize the surface dents and deformations of the panels.
- Investigate the effect of layup orientation on impact damage thresholds. Delamination is often the form of damage caused by an impact, and the layup orientation can affect a laminate's vulnerability to delamination.

7.0 References

1. International Air Transportation Association 2005, "Ground Damage Prevention Programme Targets 10% Cost Reduction," Industry Times, Edition 7, September, Article 4.
2. Kim, H. and Kedward, K. T., "Modeling Hail Ice Impacts and Predicting Impact Damage Initiation in Composite Structures," AIAA Journal, Vol. 38, No. 7, 2000, pp. 1278-1288.
3. Kim, H., Kedward, K.T., and Welch, D.A., "Experimental Investigation of High Velocity Ice Impacts on Woven Carbon/Epoxy Composite Panels," Composites Part A, Vol. 34, No. 1, 2003, pp. 25-41.
4. Rhymer, J., Kim, H., and Roach, D., "The Damage Resistance of Quasi-Isotropic Carbon/Epoxy Composite Tape Laminates Impacted by High Velocity Ice*." Composites Part A: Applied Science and Manufacturing*, DOI: 10.1016/j.compositesa.2012.02.017. Available online 3 March 2012.
5. Olsson, R., Donadon, M.V., and Falzon, B.G., "Delamination threshold load for dynamic impact on plates." *International Journal of Solids and Structures*. Vol 43, No 10, 2006, pp 3124-41.
6. Whisler, D. and Kim, H., "Effect of Impactor Radius on Low Velocity Impact Damage of Glass/Epoxy Composites," *Journal of Composite Materials*, published online 15 Feb. 2012, DOI: 10.1177/0021998312436991.